Journal of Loss Prevention in the Process Industries 68 (2020) 104323

Contents lists available at ScienceDirect

Journal of Loss Prevention in the Process Industries

journal homepage: http://www.elsevier.com/locate/jlp

An innovative and comprehensive approach for the consequence analysis of liquid hydrogen vessel explosions

Federico Ustolin [a,*], Nicola Paltrinieri [a], Gabriele Landucci [b]

[a] Department of Mechanical and Industrial Engineering, Norwegian University of Science and Technology NTNU, S.P. Andersens veg 3, Trondheim, 7031, Norway
[b] Department of Civil and Industrial Engineering, University of Pisa, Largo Lucio Lazzarino, Pisa, 56122, Italy

ARTICLE INFO

Keywords:
BLEVE
Hydrogen safety
Consequence analysis
Liquid hydrogen
Hydrogen explosion
Fireball

ABSTRACT

Hydrogen is one of the most suitable solutions to replace hydrocarbons in the future. Hydrogen consumption is expected to grow in the next years. Hydrogen liquefaction is one of the processes that allows for increase of hydrogen density and it is suggested when a large amount of substance must be stored or transported. Despite being a clean fuel, its chemical and physical properties often arise concerns about the safety of the hydrogen technologies. A potentially critical scenario for the liquid hydrogen (LH_2) tanks is the catastrophic rupture causing a consequent boiling liquid expanding vapour explosion (BLEVE), with consequent overpressure, fragments projection and eventually a fireball. In this work, all the BLEVE consequence typologies are evaluated through theoretical and analytical models. These models are validated with the experimental results provided by the BMW care manufacturer safety tests conducted during the 1990's. After the validation, the most suitable methods are selected to perform a blind prediction study of the forthcoming LH_2 BLEVE experiments of the Safe Hydrogen fuel handling and Use for Efficient Implementation (SH_2IFT) project. The models drawbacks together with the uncertainties and the knowledge gap in LH_2 physical explosions are highlighted. Finally, future works on the modelling activity of the LH_2 BLEVE are suggested.

1. Introduction

Hydrogen could be one of the options to shift the world energy production from fossil toward renewable and clean fuels. In order to be considered clean and renewable, hydrogen must be produced from non-fossil fuels such as biomass, organic material or waste, as well as from water (Ustolin et al., 2020). If hydrogen is generated from light hydrocarbons (e.g. natural gas), the carbon separation and sequestration technique must be employed to minimise the carbon dioxide emission in the atmosphere. The growth of renewable energies such as solar and wind may be supported by exploiting their surplus and producing hydrogen from water via electrolysis, as energy storage method (Maggio et al., 2019). The only by-products are water and heat when it is supplied to the fuel cells devices to produce electricity. Even when hydrogen is burnt, its combustion produces only water if the flame temperature is controlled or a catalyst is employed (Fumey et al., 2018).

After being stored, this fuel is suitable for transportation to the final users by different means thanks to its low weight (40.2 kg m^{-3} at 700 bar and 15 °C (NIST, 2019)) and high energy content (120 MJ kg^{-1} (McAllister et al., 2011)). The liquefaction process is one of the methods that can increase the hydrogen density (up to 70.9 kg m^{-3} at ambient pressure and 20.3 K (NIST, 2019)), in order to transport a larger amount. Moreover, during liquefaction, hydrogen is converted from the normal composition (75% ortho-hydrogen, 25% para-hydrogen) to 100% para-hydrogen by means of a catalyst to increase its stability and hence reduce its evaporation (Zhuzhgov et al., 2018). To further reduce the boil-off gas (BOG) rate, the liquid hydrogen (LH_2) is then stored in highly insulated tanks (Barthelemy et al., 2017). These tanks are defined as double walled since they are composed by an inner vessel inside an outer one, separated by a vacuum jacket filled with insulating material. The two most common insulation types are perlite and the multilayer insulation (MLI), i.e. polymer sheets covered with a reflecting metal such as aluminium and separated by an insulating material (e.g. fiberglass) (Peschka, 1992). The residual gas pressure in the vacuum jacket has a high impact on the heat losses. For instance, the estimated thermal conductivity of a typical MLI with a layer density of 24 layers cm^{-1} and boundary temperature of 300 and 90.5 K is almost 0.04 mW m^{-1} K^{-1} at 10^{-4} torr, while it increases up to 30 mW m^{-1} K^{-1} at 10^{2} torr (Barron and Nellis, 2016). The heat flux rate through the insulation of an LH_2 tank depends on many factors such as the type of insulation and its thickness, the residual gas pressure in the and the type of gas presents in

* Corresponding author.
E-mail address: federico.ustolin@ntnu.no (F. Ustolin).

https://doi.org/10.1016/j.jlp.2020.104323
Received 4 August 2020; Received in revised form 20 September 2020; Accepted 8 October 2020
Available online 10 October 2020

List of symbols

A_D	cross-sectional area of the fragment (m^2)
A_{ke}	fraction of mechanical energy responsible for the ejection of the fragments (kinetic energy)
A_L:	external area of the fragment plane parallel to trajectory (m^2)
$c_{p,L}$:	average specific heat at constant pressure of the liquid phase between the initial and final states (kJ kg^{-1} K^{-1})
C_D	drag coefficient of the fragment (−)
C_L:	lift coefficient of the fragment (−)
$c_{p,L0}$	specific heat at constant pressure of the liquid at boiling point (kJ kg^{-1} K^{-1})
d	distance from the tank (m)
D_{fb}	diameter of the fireball (m)
D_V	vessel diameter (m)
E_{av}	available mechanical energy (J)
E_{SEP}	surface emissive power (W m^{-2})
f	flashing fraction (−)
F_{fb}	view factor of the fireball
g	acceleration of gravity (m s^{-2})
H	vertical fragments range (m)
h_L:	specific enthalpy of the liquid phase immediately prior the explosion (kJ kg^{-1})
h_{L0}	specific enthalpy of the liquid phase at boiling point (kJ kg^{-1})
h_{V0}	specific enthalpy of the vapour phase at boiling point (kJ kg^{-1})
i_s	impulse of the pressure wave (Pa s)
k	fraction of energy converted in overpressure (−)
L:	distance between the fireball centre and the target (m)
M_C	empty mass of the vessel (kg)
M_F	mass of fragment (kg)
m_L:	mass of the liquid phase (kg)
m_V	mass of the vapour phase (kg)
m_T	mass of the whole substance contained in the tank (kg)
P	pressure before the explosion (Pa)
P_a	pressure at the final state (usually equal to P0) (MPa)
P_0	atmospheric pressure (Pa)
P_C	critical pressure (Pa)
p_s	side-on overpressure (Pa)
p_w^0	partial pressure of saturated water vapour (Pa)
R	horizontal fragment range (m)
R_{fb}	radius of the fireball (m)
RH	relative humidity of atmospheric air (%)
$\overline{R}$	: Sachs scaled distance (−)
$\overline{R}_F$	: scaled fragment range (−)
q	incident radiation of the fireball (W m^{-2})
q_L:	heat released by the liquid phase after the explosion (kJ kg^{-1})
q_V	latent heat of vaporisation (kJ kg^{-1})
s_L:	specific entropy of the liquid phase before the explosion (kJ kg^{-1} K^{-1})
s_{L0}	specific entropy of the liquid phase at boiling point (kJ kg^{-1} K^{-1})
s_V	specific entropy of the vapour liquid phase before the explosion (kJ kg^{-1} K^{-1})
s_{V0}	specific entropy of the vapour phase at boiling point (kJ kg^{-1} K^{-1})
T	temperature of the substance inside the tank before the explosion (K)
T_0	boiling point temperature (K)
T_C	critical temperature (K)
T_{fb}	fireball temperature (K)
t_{fb}	duration of the fireball (s)
T_{SL}:	superheat limit temperature (K)
U_i	overall internal energy of the system before the explosion (MJ)
u_L:	internal energy of the liquid phase before the explosion (kJ kg^{-1})
u_{L0}	internal energy of the liquid phase at boiling point (MJ kg^{-1})
u_{Lis}	internal energy of the liquid phase after the isentropic expansion (kJ kg^{-1})
u_V	internal energy of the vapour phase before the explosion (kJ kg^{-1})
u_{V0}	internal energy of the vapour phase at boiling point (MJ kg^{-1})
u_{Vis}	internal energy of the vapour phase after the isentropic expansion (kJ kg^{-1})
V^*	volume of the expanding fluid (m^3)
v_i	initial velocity of the fragments (m s^{-1})
v_{L0}	specific volume of the liquid phase at boiling point (m^3 kg^{-1})
V_T	tank volume (m^3)
v_{V0}	specific volume of the vapour phase at boiling point (m^3 kg^{-1})
x	vapour fraction after the irreversible expansion (−)
x_{fb}	distance between the release point and the target (m)
x_L:	specific entropy fraction of the liquid phase (−)
x_V	specific entropy fraction of the vapour phase (−)
W_{TNT}	TNT equivalent mass (kg_{TNT})
Z	TNT scaled distance (m $kg^{-1/3}$)
α_i	initial angle of the fragments (°)
β	fraction of mechanical energy which participates in the blast wave (−)
γ	specific heat ratio (−)
Δh_{V0}	latent heat of vaporisation at boiling point (kJ kg^{-1})
ε	emissivity of the body (−)
θ	angle between the receptor surface normal and L (°)
ρ_a	density of atmospheric air (kg m^{-3})
ρ_L:	density of the liquid phase (kg m^{-3})
ρ_V	density of the liquid phase (kg m^{-3})
σ	Stefan-Boltzmann constant (5.67×10^{-8} W m^{-2} K^{-4})
τ	atmospheric attenuation factor (transmissivity) (−)
ψ	amount of energy which participate in the generation of the pressure wave (−)

the vacuum jacket (e.g. air or nitrogen), the shape of the tank (cylindrical or spherical) as well as its size. For instance, Stochl and Knoll (1991) measured a total heat leak of 48.2 W from an LH_2 tank with a volume of 4.96 m^3, insulated with 34 layers of MLI, an external temperature of 350 K and an internal one of 20.3 K. This corresponds to an extremely low heat flux of 3.4 W m^{-2} (Stochl and Knoll, 1991). Another option to maintain the hydrogen in liquid phase would be to refrigerate the tank insulation by exploiting the extremely cold BOG. This is achieved through vapour cooled shields installed inside the vacuum jacket and composed by coils of pipes where the BOG recirculates (Peschka, 1992). In addition, zero boil-off methods for large scale liquid hydrogen tanks were recently developed by NASA. These methods exploit an integrated refrigeration and storage system (Notardonato et al., 2017).

It must be mentioned that the hydrogen liquefaction is an energy

demanding process since up to 13.3 kWh per kg of hydrogen are requested, which corresponds to approximately 30% of the hydrogen lower heating value (LHV) (Bracha et al., 1994). However, the liquid phase seems to be the only fashion to transport large amount of hydrogen over long distances, or to be store onboard of large hydrogen fuelled vehicles such as ships (NCE Maritime Cleantech, 2019). Furthermore, Cardella et al. (2017) proposed a solution to optimise the liquefaction process and thus increase its efficiency and reduce the costs. Finally, Trevisani et al. (2007) suggested to produce electricity by recovering the thermal energy during the LH_2 vaporisation process through different systems such as a gas turbine or magnetohydrodynamic generator. In this manner, the overall efficiency of the liquefaction process can be improved.

Hydrogen is extremely flammable, odourless, and colourless, making it also difficult to detect (NASA, 2005). Thus, the safety aspects are crucial for hydrogen applications, which are progressively increasing in popularity, affecting the consumption of the hazardous substance (IEA, 2019) and its supply chain (Landucci et al., 2010). For instance, the first hydrogen fuelled train was deployed in Germany in 2018 (D'Ovidio et al., 2020), and the interest for this fuel is escalating in the maritime sector (van Biert et al., 2016) (NCE Maritime Cleantech, 2019). From emerging technologies, emerging risks might arise due to the lack of experience and knowledge (Jovanović and Baloš, 2013). For this reason, the atypical accident scenarios, which are the events not considered by the most common risk assessment techniques, must be investigated (Paltrinieri et al., 2012). When a vessel of liquefied gas is used, the boiling liquid expanding vapour explosion (BLEVE) is one of the atypical accident scenarios that might manifest. BLEVE is a physical explosion since it is not led by chemical reactions, yet by a rapid phase change and expansion (CCPS, 2010). One of the most recent BLEVE definitions states that this explosion may occur after the rupture of a tank containing a liquid at a temperature above its boiling point at atmospheric pressure, due to the expansion of both the vapour and liquid phases (Casal et al., 2016).

The first consequence of a BLEVE is the pressure wave generated by the explosion. The overpressure of the blast wave can cause different types of damages on structures, injuries or even death to humans, depending on its intensity (Baker et al., 1983). Part of the mechanical energy generated by the explosion contributes to the tear the vessel and throw away its debris. In the literature, this consequence is usually called missiles, projectiles, or fragments. In this study, this latter definition was adopted.

A fireball may be initiated from a BLEVE if the stored substance is flammable and an ignition source is present outside the vessel. According to the Centre for Chemical Process Safety (CCPS, 2010), the fireball is "a burning fuel-air cloud whose energy is emitted primarily in the form of radiant heat". In addition, this cloud tends to ascend and expand while burning due to the buoyancy of the hot gases. The fireball terminology was chosen because this cloud usually assumes a spherical shape or sometime a mushroom aspect since a stem might be created between the cloud and the fuel spilled on the ground (High, 1968). Under certain circumstances, an actual fireball does not take place. Instead, a fire starts on the ground after the loss of containment. This may represent a third type of BLEVE consequence. Bader et al. (1971) studied this event circumstances and determined the critical mass of the rocket propellants above which a fireball is formed and lift off.

Many causes could provoke the collapse of the vessel. The BLEVEs have been categorised in "fired" or "unfired" depending on the cause of the loss of containment (Paltrinieri et al., 2009). The fired or hot BLEVE is induced by a thermal source external to the tank, i.e. a jet or a pool fire. In this case, the heat transfer between the surrounding and the substance in the tank is enhanced, the vessel pressure rises due to the liquid evaporation and the decrease of density. Moreover, the external thermal source reduces the mechanical resistance of the tank wall material and the tank pressure increases the stress (Paltrinieri et al., 2009). On the other hand, an unfired or cold BLEVE can be caused by a violent impact (e.g. road accident), a pressure relief valves (PRVs) failure, or a defect on the insulation material.

Few LH_2 BLEVE accidents can be found in the literature, and in most of the cases the term BLEVE is not adopted by the authors of the accident reports. An example is provided by Gayle (1964), who describes the explosion of the S-IV All Systems Vehicle occurred on January 24, 1964, at the Douglas Aircraft Company, Sacramento. The author states that this was the second known accident involving large amount of liquid oxygen (LOX) and LH_2 at that time. In the report, the focus is placed on the fireball characterisation, the fragments range analysis, and the damages on the structures closed to the test facility. After this accident and during the 1960's, numerous test series, such as the PYRO project (Willoughby and Ullian, 1988) and Atlas/Centaur abort (Kite et al., 1965), were conducted to study the explosions of different types of liquid-propellants (e.g. RP-1/LOX, LH_2/LOX). Empirical correlations for the fireball development to estimate diameter and duration after the explosion of liquid-propellants were proposed by Gayle and Bransford (1965) and High (1968). A thermal radiation model for liquid-propellants was developed by Bader et al. (1971). Prugh (1994) assessed the thermal radiation for fireballs generated after BLEVEs as well, but LH_2 was not considered due to the high temperatures and low emissivity.

An LH_2 BLEVE accident occurred on January 1st, 1974 can be also found online (HydrogenTools, 2017), but its description focuses on the causes which provoked the phenomenon, neglecting its consequences. A similar LH_2 BLEVE event is analysed by Mires (1985). In this case, the fragments range is reported as consequence and a reverse analysis is conducted to comprehend the LH_2 amount involved and the tank pressure necessary to throw the tank end cap almost 76 m (180 ft) from the vessel. In both the accidents, a cold BLEVE occurred without ignition after the release. An example of hot LH_2 BLEVE took place during the Challenger space shuttle disaster in 1986 (NASA, 1997). In particular, hot gases ignited after their release from one solid rocket booster due to the failure of an O-ring rubber seal. The flames impinged the LH_2/LOX external tank provoking its rupture and a consequent BLEVE. This accident involved the LOX tank as well as all the tests conducted by NASA for the aerospace applications previously mentioned. Despite this event has occurred at least three times in the past, it might be still neglected during a risk assessment of LH_2 technologies (Ustolin et al., 2019).

The only experiments in which the LH_2 BLEVE phenomenon was simulated, were carried out by BMW car manufacturer on few automotive LH_2 tanks, in the period 1992–95 (Pehr, 1996). Although the three main BLEVE consequences (blast wave, fragments range and fireball) were considered and measured, some critical results were omitted (Ustolin and Paltrinieri, 2020). For instance, a thorough fragments analysis was disregarded. Furthermore, it was not possible to develop an experimental model to assess the absolute thermal radiation load in the fireball proximity, and the thermal radiation results were not published. These tests are described in detailed in Sec. 3.2.

During the integrated design for demonstration of efficient liquefaction of hydrogen (IDEALHY) project, an accurate qualitative risk assessment of hydrogen liquefaction, storage and transportation was carried out (Lowesmith et al., 2013). The consequences of the fireballs generated after different large scale LH_2 BLEVEs were estimated by means of empirical correlations and a model developed by the Loughborough University to assess the fireball radiation. As result of this project, the most severe event for both the transportation/storage and liquefaction/storage scenarios was the LH_2 BLEVE. Recently, the BLEVE phenomenon was considered for LH_2 by Hansen (2020), with a comparison between the consequences of an LH_2 and a liquefied natural gas (LNG) BLEVE. Currently, the safe hydrogen fuel handling and use for efficient implementation (SH_2IFT) project is investigating the safety aspects of a loss of containment of both liquid and compressed hydrogen tanks (Ustolin et al., 2019). In particular, the consequences of an LH_2 BLEVE explosion are analysed through either experimental tests or modelling activity. Furthermore, the project is focussing on the

consequences of the release of LH_2 onto water and compressed hydrogen from high pressurized vessels.

Given these premises, the aim of this work is to present a novel approach for the comprehensive assessment of the consequences of an LH_2 BLEVE. The approach is validated and employed to conduct blind predictions for the consequences of LH_2 accident scenarios. Moreover, this method is not limited to LH_2 but it could be applied to other substances as well.

To achieve the study objective, the BMW tests are considered for the first time and simulated by means of conventional risk assessment empirical and theoretical models. The idea was to investigate if these very well-known methods already validated for hydrocarbons BLEVE (e.g. propane and butane) are suitable for LH_2 BLEVE as well. These equations were never applied to LH_2 BLEVEs before, thus the outcomes of this analysis required to be validated with the experimental results. After the validation, the most suitable models for the LH_2 BLEVE consequence analysis are selected. The chosen models are applied to conduct a blind prediction study in order to estimate the consequences of a planned experimental tests set and generalize on potential BLEVE events for LH_2 under different conditions. For the first time, this approach allows assessing all the identified typologies of BLEVE consequences for both small- and mid-scale LH_2 accident scenarios. Therefore, the novelty of this study is mainly represented by the innovative methodology which allows to validate the available consequence analysis model and conduct a blind prediction study of the BLEVE phenomenon, and by considering and simulating for the first time the BMW safety tests.

In Sec. 2, the difference between a sub- and supercritical BLEVE is explained and the para-hydrogen properties are specified. The methodology adopted in this study and the results attained are reported in Sec. 3 and 4, respectively. In-depth discussion on the results and several observations on the employed models were provided in Sec. 5, and finally the conclusion together with the suggested future works are described in Sec. 6.

2. Subcritical and supercritical BLEVEs

According to Reid (1979), the liquid must be significantly superheated to consider the explosion after the tank rupture as severe as a BLEVE. When the superheated liquid or subcooled vapour approach the superheat limit temperature (T_{SL}), their states may shift either from metastable to equilibrium state under small perturbations or to unstable due to large perturbations (Casal, 2008). Under this thermodynamic state, a homogeneous nucleation may be attained as consequence of a rapid depressurisation. Therefore, a violent expansion which characterises the explosion is the aftermath of this nucleation type. It must be noticed that during such event, also the vapour phase contained in the tank contributes to the explosion yield. According to Birk et al. (2007), the pressure shock during a propane BLEVE is generated only by the vapour phase contribution since the liquid flashing is a slow process, thus not able to generate such an overpressure. However, this latter is responsible for fragments ejection and dynamic pressure loading of structures in the near field (Birk et al., 2007). On the other hand, the model developed by Casal and Salla (2006) to estimate the blast wave overpressure, takes into account barely the liquid phase contribution.

Table 1
Thermodynamic properties of parahydrogen.

Property	Value	Units
Boiling temperature (T_0)	20.277	K
Critical temperature (T_C)	32.938	K
Critical pressure (P_C)	12.838	bar
Enthalpy of vapour @ BP[a] (h_{V0})	445.4	kJ/kg
Enthalpy of liquid @ BP[a] (h_{L0})	-6.1×10^{-13}	kJ/kg

[a] BP: boiling point.

It might happen that during an accident, the substance contained in the vessel reaches the status of either compressible liquid or supercritical fluid due to the rise in pressure and temperature. Hence, the liquid and vapour phases are not present anymore. This can be caused by different events such as a fire external to the vessel or a defect in the tank insulation of the cryogenic tanks, leading to an undesired heat transfer between the substance and the surrounding. Therefore, if the catastrophic rupture of the vessel is attained when the status of the fluid is supercritical, the consequent explosion is called supercritical BLEVE (Laboureur, 2012; Laboureur et al., 2014, 2012a; 2012b; Zhang et al., 2016). Hydrogen has a low critical pressure (12.964 bar (NIST, 2019)) and an extremely low critical temperature (33.145 K (NIST, 2019)) compared with other substances and conventional fuels (hydrocarbons). For this reason, a supercritical BLEVE seems a likely scenario for a LH_2 tank. In this study, if the pressure and temperature inside the tank are lower than the critical point immediately prior the explosion the BLEVE is called subcritical, otherwise the explosion is referred as a supercritical BLEVE. The compressible liquid status is not covered in this paper because it is assumed that pressure and temperature of the substance inside the vessel follow the saturation curve before the critical point.

2.1. Para-hydrogen properties

As mentioned before, hydrogen is converted to para-hydrogen (p-H_2) during the liquefaction process in order to increase its stability and thus reduce the boil off (spontaneous evaporation) (Zhuzhgov et al., 2018). For this reason, only the properties of p-H_2 were considered in this study. Similarly to hydrogen, p-H_2 has a low critical pressure, (12.8377 bar (NIST, 2019)) and an extremely low critical temperature, (32.938 K (NIST, 2019)). In Table 1, the thermodynamic properties of p-H_2 are collected.

3. Methodology

3.1. Superheat limit temperature (T_{SL}) estimation for para-hydrogen

As described in Sec. 2, the superheat limit temperature aids to determine if the explosion may be considered as a BLEVE. The T_{SL} is directly affected by the critical point of the substance. Thus, the T_{SL} of p-H_2 (see Table 1) notably differs from most of the conventional fuels as well. In the scientific literature, many methods to estimate the superheat limit temperature are proposed (Casal, 2008). In this work, the p-H_2 T_{SL} is calculated with three of the most representative models. These approaches were selected because they generally provide the highest, the lowest and the average values of the superheat limit temperature (Casal, 2008).

1. The first one is proposed by Reid (1976) and consists in a widely used correlation with the critical temperature (Eq. (1)):

$$T_{sl-T_C} = 0.895 \cdot T_C \quad (1)$$

This equation derives from bubble-column experiments conducted at different pressures for di-chlorodifluoromethane, n-pentane, n-hexane, n-heptane, and cyclohexane (Reid, 1976). It was demonstrated that for these substances, the T_{SL} at atmospheric pressure was 0.89–0.90 times the critical temperature. In the following, this model is called Experimental Correlation (EC).

2. The second method, described by Casal (2008), estimates the T_{SL} from the tangent to the saturation curve at the critical point ($T_{SL\text{-}t}$). Although this approach is not based on any thermodynamic law or equation, it is one of the most conservative methods (Casal, 2008). In this study, the tangent line was built graphically in order to avoid the significant error given by the Clausius-Clapeyron equation close to the critical point (CP) (Casal, 2008). The temperature intercepted by the tangent at ambient temperature (P_0) is the $T_{SL\text{-}t}$. In particular, this temperature was estimated with the straight line equation (Eq. (2)):

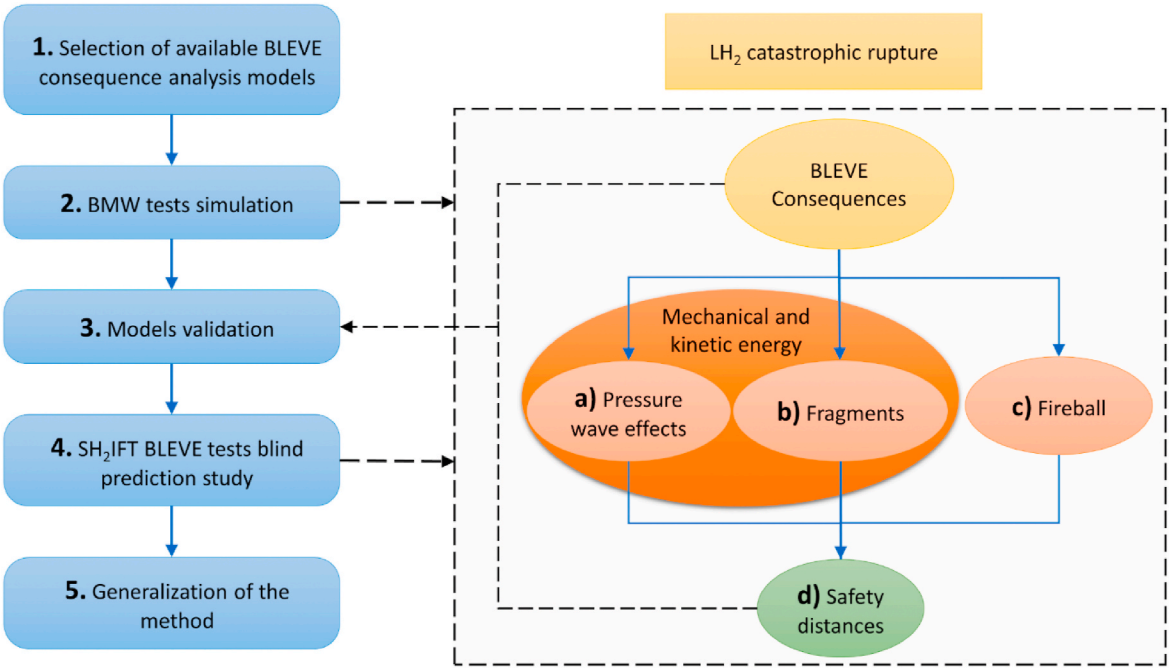

Fig. 1. Methodology steps and approach applied in the LH_2 consequence analysis.

Table 2
Equations of the ideal gas behaviour models selected in this study.

Proposed by	Assumption	Equation	
Brode (1959)	Isochoric process	$E_{Brode} = \frac{P - P_0}{\gamma - 1} V^*$	(5)
Smith and Van Ness (1996)	Isothermal process	$E_{IE} = P \cdot V^* \cdot \ln \frac{P}{P_0}$	(6)
Crowl (1992, 1991)	Thermodynamic availability	$E_{TA} = P \cdot V^* \left[\ln\left(\frac{P}{P_0}\right) - \left(1 - \frac{P_0}{P}\right) \right]$	(7)
Prugh (1991)	Adiabatic process	$E_{Prugh} = \frac{P \cdot V^*}{\gamma - 1}\left(1 - \frac{P_0}{P}\right)^{\frac{\gamma - 1}{\gamma}}$	(8)

$$P = \tan\alpha \cdot T + b \quad (2)$$

where the gradient is the tangent of the angle α, and the intercept b was determine at CP, replacing the pressure and temperature with P_C and T_C respectively. This model is called Saturation Curve Tangent (SCT) in this study.

3. The third method, proposed by Salla et al. (2006), estimates the T_{SL} through an energy balance. An adiabatic vaporisation process is considered after the depressurisation of the vessel in which part of the liquid cools down to the boiling point (T_0) at atmospheric pressure releasing a certain amount of heat ($q_L = h_L - h_{L0}$), partially or totally absorbed by a liquid fraction which vaporises. The $T_{SL\text{-}E}$ is the temperature at which the heat released by 50% of the liquid (q_L) is equal to the heat required by the other half of the liquid ($q_V = h_{V0} - h_L$) to vaporise. The $T_{SL\text{-}E}$ is then the temperature correspondent to h_L on the saturated liquid line. This model was named Energy Balance (EB) in the following.

3.2. Approach for the comprehensive consequences assessment of an LH_2 BLEVE

The LH_2 BLEVE is studied and physically modelled in this work. In particular, the most significant consequence analysis models were selected (step 1 in Fig. 1) in order to create a suitable approach to assess the LH_2 BLEVE consequences. This approach is depicted by the black rectangle in Fig. 1 and it foresees to estimate the safety distance from the tank, from the results of the three main BLEVE consequences.

Then, the BMW safety tests were simulated (step 2) with the aforementioned approach. Therefore, a first validation of the chosen methods was possible (step 3). Hence, a blind prediction was accomplished by applying the same approach to the conditions of the LH_2 BLEVE tests which will be carried out during the SH_2IFT project. In this way, it was shown how the proposed methodology can be applied to future LH_2 BLEVE consequence analysis. In the following, the models and the steps adopted for the consequence analysis are described.

3.3. Model selection and consequence analysis approach

In this section, the models selected for the consequence analysis (step 1 in Fig. 1) are described, together with the approach proposed to estimate the safety distance from the tank (black dashed rectangle of

Table 3
Equations of the real gas behaviour models selected in this study.

Proposed by	Equation	
van den Bosch and Weterings (2005)	$E_{TNO} = m_V (u_V - u_{V_{is}}) + m_L (u_L - u_{L_{is}})$	(9)
Planas-Cuchi et al. (2004)	$E_{Planas} = -[(u_{L0} - u_{V0}) m_T \cdot x - m_T \cdot u_{L0} + U_i]$	(10)
Casal and Salla (2006)	$E_{SE} = k \cdot m_L (h_L - h_{L0})$	(11)
Genova et al. (2008)	$E_{Genova} = \psi \cdot m_L \cdot c_{p,L} (T_L - T_{L0})$	(12)
Birk et al. (2007)	$E_{Birk} = m_V (u_V - u_{V_{is}})$	(13)

Fig. 1). The idea is to use the results of the three main BLEVE consequences to determine this distance. In the following, the mechanical energy models adopted to evaluate the pressure wave effects and the fragments range are reported together with the overpressure, impulse, fragments range and fireball models. It must be mentioned once again that these models have not been employed to LH_2 before, hence a verification with the experimental results is required.

3.3.1. Mechanical energy models

The approach proposed by (Hemmatian et al., 2017a) was adopted to estimate the mechanical energy generated by the explosion in order to determine the severity of the pressure wave (overpressure and impulse). This procedure foresees to compare different mechanical energy models. The ideal gas behaviour models proposed by the following authors were considered in this study:

1. Brode (1959);
2. Smith and Van Ness (1996);
3. Crowl (1992, 1991), thermodynamic availability (TA) model;
4. Prugh (1991).

These models, described below, depends only on the atmospheric and tank pressures, and the volume of the expanding fluid. The equations of the selected models are reported in Table 2, where P and P_0 are the pressure inside the tank immediately prior the explosion and the atmospheric pressure respectively, in P_a, γ is the heat specific ratio (1.4 for hydrogen) and V^* is the sum of the vapour and flashing liquid fraction volumes in m^3 at subcritical conditions, and the total tank volume (V_T) at supercritical conditions. Prugh (1991) suggested the following method to estimate the total expansion volume (vapour and liquid fractions) during the explosion of a container of liquefied gas. The total volume is calculated with Eq. (3) at subcritical conditions:

$$V^* = V_T + m_L\left(\frac{f}{\rho_V} - \frac{1}{\rho_L}\right) \tag{3}$$

where V_T is the total volume of the tank in m^3, m_L is the mass of the liquid in kg, ρ_V and ρ_L are the density of the vapour and liquid phase respectively in kg m^{-3}, and f is the flashing fraction estimated with Eq. (4):

$$f = 1 - \exp\left\{-2.63\left[1 - \left(\frac{T_C - T_0}{T_C - T_b}\right)^{0.38}\right]\frac{c_{p,L0}}{\Delta h_{V0}}(T_C - T_b)\right\} \tag{4}$$

where T_0, T_C and T_b are the atmospheric, critical and boiling temperatures respectively in K, $c_{p,L0}$ is specific heat of the liquid at boiling temperature in kJ kg^{-1} K^{-1}, and Δh_{V0} is the latent heat of vaporisation at boiling point in kJ kg^{-1}. It must be emphasized that when the substance in the vessel reaches supercritical conditions before the explosion, V^* is equal to the total tank volume (V_T) in m^3.

Brode (1959) proposed Eq. (5) to estimate the total energy generated by the detonation of a spherical charge of TNT considering it as an isochoric process. Smith and Van Ness (1996) assumed an isothermal expansion (IE) process while developing their model (Eq. (6)). The thermodynamic availability (TA) model introduced by Crowl (1992, 1991) estimates the maximum mechanical energy extractable from a substance which reversibly reaches the equilibrium with the surrounding environment from the burst conditions. Eq. (7) can be used when the process is considered isothermal. Prugh (1991) proposed to apply Eq. (8), developed for high pressure containers to liquefied gas vessels by replacing the tank volume with the total volume of the expanding fluid (Eq. (4)) in order to determine the mechanical energy of a BLEVE explosion. The fluid is considered always as ideal and the process as adiabatic.

Furthermore, the following real gas behaviour models were utilised in this study and described below:

5) van den Bosch and Weterings (2005), TNO model;
6) Planas-Cuchi et al. (2004);
7) Casal and Salla (2006), superheating energy (SE) model – isentropic and irreversible processes;
8) Genova et al. (2008);
9) Birk et al. (2007).

The formulae of these models are collected in Table 3, where m, u, h, T, U_i and $c_{p,L}$ refer to the masses in kg, internal energies in kJ kg^{-1} (except for the Planas model where the units are MJ kg^{-1}), the enthalpies in kJ kg^{-1}, the temperatures in K, the overall internal energy of the system before the explosion in MJ and the average specific heat at constant pressure of the liquid phase between the initial and final states of the expansion in kJ kg^{-1} K^{-1}. Moreover, the indexes V, V_0, L, L_0 indicates the vapour and liquid phases before and after (at atmospheric pressure) the explosion, respectively, while T and is refer to both liquid and vapour phases (total) and the isentropic process, respectively.

The TNO model (van den Bosch and Weterings, 2005) in Eq. (9) considers the expansion of both the vapour and liquid phases, and assumes that this is an isentropic process. The thermodynamic properties are usually retrieved from a suitable database at saturation conditions. The specific internal energies after the isentropic expansion, u_{Vis} and u_{Lis} in kJ kg^{-1}, are estimated with Eqs. (14) and (15) reported in Table 4, where the ratios x_V and x_L are assessed with Eqs. (16) and (17), and s indicates the entropies of the vapour and liquid phases before and after the explosion in kJ kg^{-1} K^{-1}.

Planas-Cuchi et al. (2004) suggested a method which acknowledge that the explosion is an adiabatic irreversible process. The equation of this model is reported in Eq. (10), where x is the intersection point between two equations: the variation in internal energy (ΔU) and the adiabatic irreversible expansion work ($P_0 \cdot \Delta V$). Eq. (18) in Table 4 is employed to estimate the value of x, where P_a is the pressure at the final state (usually equal to P_0) in MPa, v_{V0} and v_{L0} are the specific volumes of the vapour and liquid phases respectively in m^3 kg^{-1}. The authors of this model assume that only part of the mechanical energy contributes to the pressure wave, i.e. 80% if the tank ruptures in a fragile manner, or 40% the type of failure is ductile (Casal et al., 2001). It should be mentioned that these latter models (TNO and Planas) can be employed to barley estimate a subcritical BLEVE since both phases (vapour and liquid) are considered. The superheating energy (SE) model (Casal and Salla, 2006) directly assess the energy contribution to the pressure wave instead of

Table 4
Internal energies and entropy ratios employed in the TNO model, and the intersection point between the variation of internal energy and the adiabatic irreversible expansion work (x) used in the Planas model.

Equation	
$u_{V_{is}} = (1 - x_L)\, u_{L0} + (x_L \cdot u_{V0})$	(14)
$u_{L_{is}} = (1 - x_V)\, u_{L0} + (x_V \cdot u_{V0})$	(15)
$x_V = \frac{s_V - s_{L0}}{s_{V0} - s_{L0}}$	(16)
$x_L = \frac{s_L - s_{L0}}{s_{V0} - s_{L0}}$	(17)
$x = \frac{m_T \cdot P_a \cdot v_{L0} - V_T \cdot P_a + m_T \cdot u_{L0} - U_i}{[(u_{L0} - u_{V0}) - (v_{V0} - v_{L0})\, P_a]\, m_T}$	(18)

Table 5
Values of the coefficients of the real gas behaviour models.

Model	β	K	ψ
TNO (van den Bosch and Weterings, 2005)	2.0	–	–
Planas-Cuchi et al. (2004)	0.4	–	–
(Casal and Salla, 2006) – isentropic proc.	1.0	0.14	–
(Casal and Salla, 2006) – irreversible proc.	1.0	0.05	–
Genova et al. (2008)	1.0	–	0.07
Birk et al. (2007)	2.0	–	–

Table 6
Multipliers for overpressure for cylindrical vessel at different $\overline{R}$ (van den Bosch and Weterings, 2005).

$\overline{R}$	
>1.6 and ≤ 3.5	1.6
>3.5	1.4

the total mechanical energy. This energy is estimated considering the enthalpy variation of only the liquid phase and its mass (Eq. (11)). The overpressure energy of either an isentropic or an irreversible process are estimated by assuming different values of the coefficient k in the model equation, i.e. 0.14 and 0.05 respectively. If this model is employed to simulate a supercritical BLEVE, the total mass of the fluid inside the tank must be considered, as well as the enthalpy of the fluid before (at supercritical conditions) and after the explosion. Similarly to the SE model, the method developed by Genova et al. (2008) takes into account only the liquid phase. The model assumes that the flashing liquid process is led by the excess heat stored in the vessel, determined with Eq. (12), where ψ is the amount of energy which participate in the pressure wave generation. This coefficient was determined empirically for propane BLEVEs and it is equal to 0.07. Genova et al. (2008) suggested to neglect the variation of the specific heat at constant pressure of the liquid ($c_{p,L}$) due to the increase in temperature since these are usually very small (less than 1% for water between 25 and 100 °C). Instead, the change in $c_{p,L}$ is significant for hydrogen (from 9.7 to 70.2 kJ kg^{-1} K^{-1} at 20.3 and 32.0 K respectively). For this reason, an average c_p value was estimated between the initial and final conditions (prior and after the explosion). The model proposed by Birk et al. (2007) is similar to the TNO model since a real gas behaviour and an isentropic expansion process are considered, but this is limited to the vapour phase. The model equation is presented in Eq. (13).

3.3.1.1. Blast wave overpressure and impulse estimation. The TNT equivalent mass method was employed both for the overpressure and impulse estimation since is the most conservative and only the far field was considered to determine the safety distance from the bursting vessel. Thus, the mechanical energies estimated with the models described above were converted in TNT masses by considering that 4680 kJ is equivalent to 1 kg of TNT (Salla et al., 2006). As previously mentioned, some models foresee that only part of the mechanical energy, hence TNT mass, contribute to the blast wave (Casal and Salla, 2006; Genova et al., 2008; Planas-Cuchi et al., 2004). On the other hand, the TNO and Birk models consider the reflection on the ground of the pressure wave, thus multiply the estimated energy (or the TNT mass) by a factor of 2. The Sachs scaled distance, estimated with Eq. (19), is usually applied to distinguish the near to the far field (Birk et al., 2007). In particular, the near field can be found when $\overline{R} < 2$.

$$\overline{R} = d\left(\frac{P_0}{\beta \cdot E}\right)^{1/3} \tag{19}$$

where d is the distance from the tank in m, P_0 is the atmospheric pressure in Pa, E is the mechanical energy estimated with one of the previously described models, and β is the fraction of energy which participates in the blast wave. In this study, the β factor was considered equal to 1 for the ideal gas behaviour models, while the values of the coefficients adopted for the real gas behaviour models are collected in Table 5.

The TNT scaled distance in m kg$^{-1/3}$, necessary to determine the overpressure and impulse from the TNT decay curve, is reported in Eq. (20):

$$Z = \frac{d}{(\beta \cdot W_{TNT})^{1/3}} \tag{20}$$

where d is the distance from the centre of the explosion, W is the TNT equivalent mass in kg, and β is the fraction of energy which participates in the blast wave.

As mentioned above, only the far field ($\overline{R} > 2$) was considered in this study. Therefore, the equation proposed by Kinney and Graham (1985) can be employed to estimate the overpressure from the TNT scaled distance.

$$\frac{p_s}{P_0} = \frac{808\left[1 + \left(\frac{Z}{4.5}\right)^2\right]}{\sqrt{1 + \left(\frac{Z}{0.048}\right)^2}\sqrt{1 + \left(\frac{Z}{0.32}\right)^2}\sqrt{1 + \left(\frac{Z}{1.35}\right)^2}} \tag{21}$$

where p_s is the overpressure in Pa, P_0 is the atmospheric pressure in Pa and Z is the TNT scaled distance in m kg$^{-1/3}$. The impulse of the pressure wave was determined with a correlation proposed again by Kinney and Graham (1985), here reported in Eq. (22):

$$i_s = \frac{6.7\sqrt{1 + \left(\frac{Z}{0.23}\right)^4}}{Z^2\sqrt[3]{1 + \left(\frac{Z}{1.55}\right)^3}} W_{TNT}^{1/3} \tag{22}$$

where Z is the TNT scaled distance in m k$^{-1/3}$ and W_{TNT} is the equivalent mass of TNT in kg. the impulse is then determined in Pa s. Ullah et al. (2017) compared different methods to estimate the impulse of the blast wave and stated that the difference in the results of these correlations diminishes when $Z > 1$. It must be noticed that the TNO and Birk models take into account the influence of the tank geometry on the blast wave. The pressure wave has a different yield along the transversal and longitudinal axes when a cylindrical vessel fails, especially in the near field (Birk et al., 2007). In Table 6, the values of the multipliers to adjust the overpressure values according to the geometry effects are collected.

Finally, according to these two models, the overpressure should by multiply by 1.1 when $\overline{R} \geq 1$ and the tank is slightly elevated above the ground (van den Bosch and Weterings, 2005).

To determine the safety distance from a vessel, both overpressure and impulse must be taken into account. Molkov and Kashkarov (2015) adopted the data published for high explosives by Baker et al. (1983) to determine the harm effects on humans from high-pressure tank explosions. In this analysis, a similar approach was selected by considering only the overpressure and impulse threshold to avoid any kind of injuries on humans and damages on structures, correspondent to 1.35 kPa and 1 Pa s. This is a conservative threshold and was adopted to determine the safety distance from the tank due to the pressure wave effects. Moreover, an overpressure threshold to avoid injuries on humans caused directly by the pressure wave was set at 16.5 kPa by Molkov and Kashkarov (2015) and here employed when only the overpressure is considered.

3.3.1.2. Fragments range. The correlation suggested by (Birk, 1996) to estimate the horizontal range of the fragments of a propane tank during a BLEVE explosion was implemented in this work. This correlation, reported in Eqs. (23) and (24), depends only on the mass of the substance contained in the vessel (m_T) and its volume (V_T).

$$R = 90 \cdot m_T^{0.33} for VT < 5m^3 \tag{23}$$

$$R = 465 \cdot m_T^{0.1} for VT > 5m^3 \tag{24}$$

Since this method usually overestimates the fragments range, the methodology proposed by CCPS (2010) was adopted in this consequence analysis as well. The initial velocity of the fragments is estimated with the correlation presented by Baum (1984) in Eq. (25):

$$v_i = \sqrt{\frac{2 \cdot A_{ke} \cdot E_{av}}{M_C}} \tag{25}$$

where E_{av} is the available mechanical energy usually estimated with the most conservative methods (IE or TNO models) in J, A_{ke} is the portion of energy responsible for the fragments ejection (kinetic energy) equal to 0.04 for the BLEVE explosion (van den Bosch and Weterings, 2005), and M_C is the empty mass of the vessel in kg. This second approach neglects the fluid dynamic forces (lift and drag) since the fragment characteristics (mass, dimensions, and shape) are usually difficult to gather or determine a priori. Eqs. (26) and (27) were utilised to calculate the horizontal (R) and vertical (H) ranges of the fragments respectively:

$$R = \frac{v_i^2 \cdot \sin(2 \cdot \alpha_i)}{g} \tag{26}$$

$$H = \frac{v_i^2 \cdot \sin(\alpha_i)^2}{2 \cdot g} \tag{27}$$

where v_i is the initial velocity of the fragments previously estimated in m s^{-1}, α_i is the initial angle of the fragments ($5 \div 10°$ for cylindrical vessels horizontally placed (CCPS, 2010)), and g is the acceleration of gravity (9.81 m s^{-2}). If the tank is placed vertically, an angle of 45° can be assumed as in (Gayle, 1964). Moreover, a third approach which instead considers the fluid dynamic force was adopted. The scaled velocity is estimated with Eq. (28):

$$\overline{v}_i = \frac{\rho_a \cdot C_D \cdot A_D \cdot v_i^2}{M_F \cdot g} \tag{28}$$

where ρ_a is the atmospheric air density (1.229 kg m^{-3} at 15 °C, 101.3 kPa (NASA, 2020)), C_D is the drag coefficient of the fragment and A_D is its cross-sectional area in m^2, v_i is again the initial velocity estimated with Eq. (25) in m s^{-1}, M_F is the fragment mass in kg, and g the gravitational acceleration in m s^{-2}. Once the scaled velocity is estimated, the scaled range is determined with the aid of a graph published by Baker et al. (1983). The horizontal fragment range (R) is then calculated from Eq. (29):

$$\overline{R}_F = \frac{R \cdot \rho_a \cdot C_D \cdot A_D}{M_F} \tag{29}$$

where $\overline{R}_F$ is the scaled fragment range. The assumption that the tank ruptures in two pieces (end caps) was made. The end caps have hemispherical shape, hence $C_D \cdot A_D = 0.615 \cdot \pi / 4 \cdot D_V^2$, where D_V is the vessel diameter in m and the tumbling of the fragment is considered, and the ratio $C_D \cdot A_D / C_L \cdot A_L = 0$ (van den Bosch and Weterings, 2005). This latter is used to select the curve on the chart provided in (Baker et al., 1983). The safety distance from the tank due to the fragments is then determined according to the most conservative fragments range result. In the following, the second and third methods are indicated as NFF (neglecting fluid dynamic forces) and CFF (considering fluid dynamic forces), respectively.

3.3.2. Fireball dimension, duration and radiation

Hydrogen is a highly flammable substance. After an LH_2 BLEVE, the formation of a fireball is a likely phenomenon, especially in the case of a hot BLEVE since the ignition source is already present externally to the tank. However, a fireball may be generated after a cold BLEVE as well due to the very low hydrogen ignition energy (0.017 mJ (Ono et al., 2007)). For instance, a spark has sufficient energy to ignite a hydrogen-air mixture, and this ignition source may be provoked during the rupture of the vessel. For this reason, the fireball dimensions (diameter and height), duration and radiation were estimated in this consequence analysis. The fireball diameter (D_{fb}) was calculated with Eq. (30) (Hord, 1972) which depends only on the total mass of the substance (m_T) in kg:

$$D_{fb} \approx 7.93 \cdot m_T^{1/3} \tag{30}$$

One of the most conservative equations to determine the height of the fireball centre (H_{fb}), provided by Bagster and Pitblado (1989), was adopted in this analysis:

$$H_{fb} = 2 \cdot R_{fb} \tag{31}$$

where R_{fb} is the fireball radius in m. A comparison between both the momentum-dominated (Eq. (32)) and buoyancy-dominated fireball formula (Eq. (33)) was conducted in order to estimate the minimum and maximum fireball duration (t_{fb}) (Beyler, 2016).

$$t_{fb} = 0.45 \cdot m_T^{1/3} \tag{32}$$

$$t_{fb} = 2.60 \cdot m_T^{1/6} \tag{33}$$

In (CCPS, 2010), the employment of the momentum-dominated fireball equation is suggested if the mass of the substance is lighter than 30,000 kg. However, Zalosh and Weyandt (2005) better estimated the duration of the fireball experimentally initiated after the rupture of a compressed tank with a volume of 72.4 L and containing 1.64 kg of hydrogen at 35.7 MPa with the second equation rather than the first one. The radiation from the fireball was assessed through the solid flame model (CCPS, 2010) in which the fireball is approximated as a homogenous sphere. The fuel contribution to the fireball is usually a critical and challenging aspect to determine. According to (Gayle and Bransford, 1965), almost the whole LH_2 amount was completely consumed during the experiments of the Pyro project (Willoughby and Ullian, 1988). For this reason, it was assumed that 100% of the LH_2 mass contributes to the fireball. The incident radiation, q, which is the radiation received by a target in W m^{-2}, was calculated with Eq. (34):

$$q = F_{fb} \cdot E_{SEP} \cdot \tau \tag{34}$$

where F_{fb} is the view factor, E_{SEP} is the surface emissive power (*SEP*) in W m^{-2}, and τ is the atmospheric attenuation factor (transmissivity). The *SEP* is usually measured during the experiments, and Johnson et al. (1991) reported a *SEP* value up to 350 kW m^{-2} for industrial size (>1000 kg) butane and propane BLEVE fireballs. This value is usually adopted for a conservative estimation. However, the fireball *SEP* is highly affected by the substance type and amount, and the tank pressure prior the release. In addition, the *SEP* is not constant on the fireball surface and during its duration. For these reasons, the *SEP* was theoretically assessed with the Stefan-Boltzmann's law (Eq. (35)).

$$E_{SEP} = \varepsilon \cdot \sigma \cdot T_{fb}^4 \tag{35}$$

where ε is the emissivity of the body, σ is the Stefan-Boltzmann constant (5.67×10^{-8} W m^{-2} K^{-4}), and T_{fb} is the fireball temperature in K. The fireball was considered as a black body ($\varepsilon = 1$) in order to obtain the most conservative estimation. The fireball temperature value was set equal to the stochiometric combustion temperature of hydrogen in air (2321 K (NASA, 2005)), since this value was assumed by Pehr (1996) as the peak temperature of the hydrogen fireballs. A similar procedure was adopted by High (1968) to estimate the thermal radiation from a Saturn V fireball where the highest temperature was 2400 K. When the distance between the release point and the target (x_{fb}) is longer than the fireball radius (R_{fb}), the view factor was estimated with Eq. (36):

$$F_{fb} = \left(\frac{R_{fb}}{L}\right)^2 \cos \vartheta \tag{36}$$

where L is the distance between the fireball centre and the target in m, and θ is the angle between the receptor surface normal and L in degree. It must be noticed that the higher value of F_{fb} is attained when this angle is zero, i.e. the receptor is completely facing the fireball and receiving its radiation. In order to obtain a conservative result, $cos(\theta)$ was assumed to

Table 7
Summary of the BMW safety tests results (Pehr, 1996).

BLEVE consequence		Test								
		2	3	4	5	6	7	8	9	10
Tank pressure (bar)		4.0	11.0	2.1	15.0	3.7	2.0	4.0	11.0	11.3
Overpressure (mbar)		110	470	33	150	60	167	77	133	150
Fragments range (m)		>15								
Fireball	Max. diameter (m)	20								
	Max. height (m)	20								
	Longest duration (s)	4								

Table 8
Characteristics of the LH_2 tanks selected for the consequence analysis.

Case study	Type	Insulation	Orientation	V_T (m^3)	M_C (kg)
BMW test (Pehr, 1996)	Single walled	Foam	Horizontal	0.12	60
SH_2IFT project	Double walled	Vacuum jacket + perlite or MLI*	Horizontal and vertical	1.00	730 (MLI), 1015 (perlite)

Notes: *MLI: multi-layer insulation.

Table 9
Initial conditions of the consequence analysis.

Simulation	LH_2 mass (kg)	Tank pressure before the explosion (bar)	Distance between the first pressure sensor and the tank (m)
BMW test (Pehr, 1996)	1.8 ÷ 5.4	2.0 ÷ 14.8	3.0
SH_2IFT project	35.4	14.0 ÷ 34.0	10.0

be equal to 1. Finally, the air transmissivity was determined with Eq. (37) (van den Bosch and Weterings, 2005):

$$\tau = 2.02 \cdot \left(RH \cdot p_w^0 \cdot \left(L - R_f\right)\right)^{-0.09} \quad (37)$$

where RH is the relative humidity (50% in this analysis), p_w^0 is the partial pressure of saturated water vapour (1705 Pa at 15 °C (van den Bosch and Weterings, 2005)), R_{fb} is the fireball radius in m, and L is the distance from the fireball centre to the target in m. The injuries caused by the fireball radiation are affected by the thermal dose which depends on the incident radiation and the exposure time to the fireball. The thermal dose was then assessed with Eq. (38):

$$Thermal\ dose = q^{4/3} \cdot t_{fb} \quad (38)$$

where q is the incident radiation in W m^{-2}, and t_{fb} is the fireball duration in s. The thermal dose threshold to avoid any kind of injuries is 80 (kW $m^{-2})^{4/3}$ s (Rew, 1997). The thermal dose was evaluated at difference distance from the fireball centre and this thermal dose was used as reference value to determine the safety distance due to the radiation emitted by the fireball. Finally, the safety distance from the failing vessel was determined by considering the longest distance among the ones previously determined due to the pressure wave, fragments range and fireball.

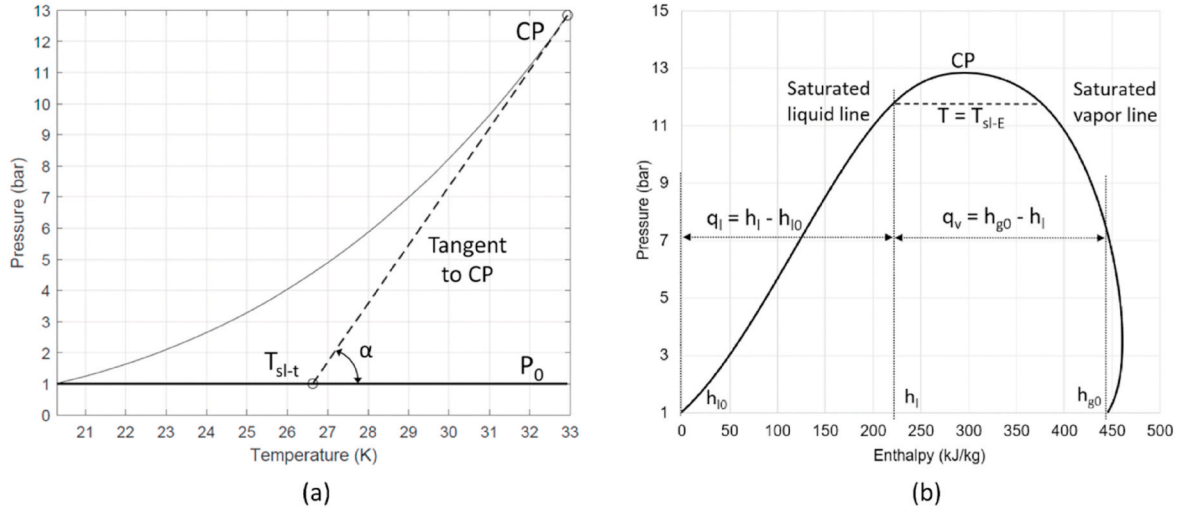

Fig. 2. (a) tangent to the parahydrogen saturation curve obtained from the application of the SCT model and (b) P-h diagram of parahydrogen obtained after the application of the EB model.

Table 10
Estimated superheat limit temperature (T_{SL}) for hydrogen.

Models	T_{SL} (K)	P (bar)
EC	29.5	7.6
SCT	26.2	4.2
EB	32.4	11.9

3.4. BMW tests simulation and validation of the models

In the period 1992–1995, a safety research program on LH_2 tanks developed for automotive application was conducted by BMW car manufacturer in cooperation with the tank manufacturers Messer Griesheim GmbH, Linde AG and other relevant licensing and research

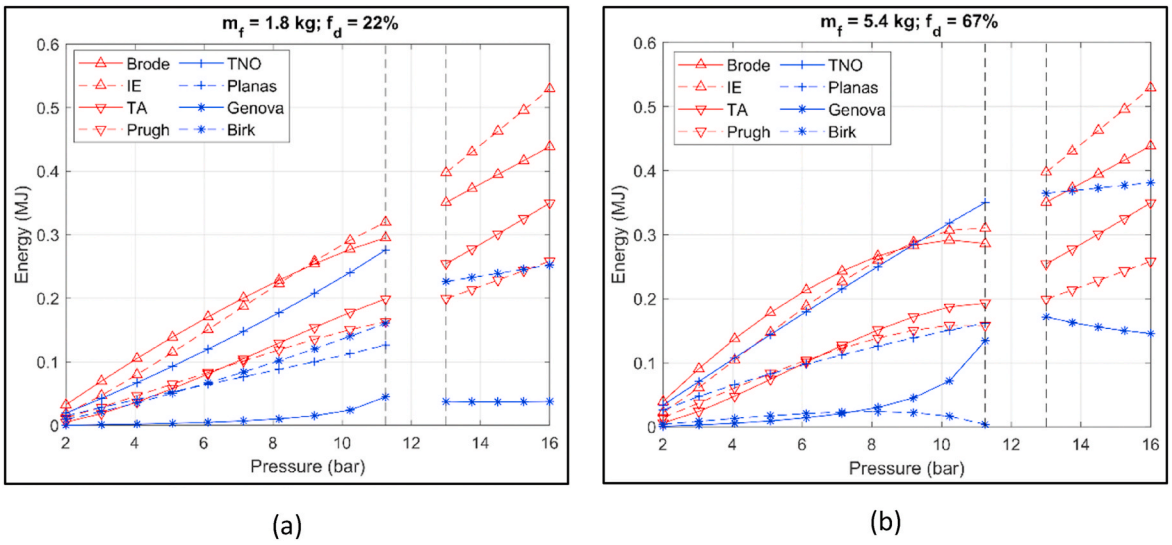

Fig. 3. Mechanical energy generated by BLEVE explosion at different tank pressures of a 0.12 m^3 tank containing (a) 1.8 kg and (b) 5.4 kg of LH_2, estimated by ideal (red) and real (blue) gas behaviour models. (For interpretation of the references to colour in this figure legend, the reader is referred to the Web version of this article.)

institutions (Pehr, 1996). Among different test types such as dynamic vibration, crash and skid, vacuum loss and fire tests (Rybin et al., 2005), the bursting tank scenario was investigated (Pehr, 1996). During this test series, ten single walled vessels with a volume of 0.120 m^3 insulated with a layer of foam and filled with different amounts of LH_2 (1.8 ÷ 5.4 kg) were wrecked at different internal pressures (2 ÷ 14.8 bar) by means of cutting charges. The description of this type of experiment corresponds to a cold BLEVE. The approach previously described was applied to simulate this case study (step 2 in Fig. 1). The results from the simulations were compared with the ones published in (Pehr, 1996) in order to validate the method for LH_2 BLEVE (step 3 in Fig. 1). The results of the BMW safety tests are collected in Table 7. During this phase, it was possible to determine which are the most suitable models for the LH_2 BLEVE consequence analysis.

3.5. Blind prediction and generalization of the method

A blind prediction is usually carried out when the experimental results are not available yet. The estimation of the consequences before the experiments may be useful to comprehend which type of instrumentation is required to record the pressure wave and fireball effects, and where it should be placed. Furthermore, a blind prediction of the BLEVE formation can determine the time to failure of the vessel, but this was not covered in this study. Finally, the predictive capabilities of the models employed in the blind prediction can be assessed by comparing its results with the experimental outcomes (Skjold et al., 2019). Different blind predictions were conducted for the consequences of hydrogen tests in the past (Skjold et al., 2019). In this work, a blind prediction of the SH_2IFT tests consequences was conducted (step 4 in Fig. 1) by employing the models selected after the validation.

During the SH_2IFT project, three double walled vessels filled at 50% with LH_2 will be engulfed in a propane fire. The tanks will be placed either horizontally or vertically and the insulations will be composed by both perlite powder and MLI inside the vacuum jackets in different tests. The pressure relief valves (PRVs) installed on the tanks will be closed to simulate a device failure. The experiment is foreseen to last until the

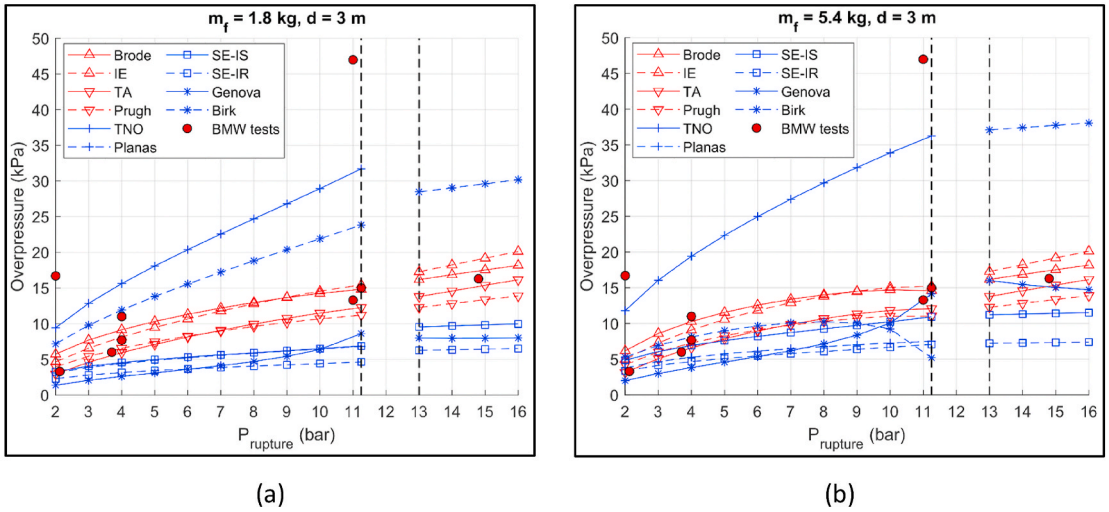

Fig. 4. Overpressure from the blast wave at 3 m from a sub- and supercritical BLEVE of a tank containing (a) 1.8 kg and (b) 5.4 of LH_2. Red circles indicates the overpressures measured during the BMW safety tests (Pehr, 1996). (For interpretation of the references to colour in this figure legend, the reader is referred to the Web version of this article.)

collapse of the vessels. In this manner, a hot BLEVE will be simulated if proper thermodynamic conditions will be reached inside the container. Since the bursting pressure is unknown, it was determined with the procedure proposed by Casal (2008). The failing pressure in the worst-case scenario should be four times the design pressure. According to (Rybin et al., 2005), the maximum allowable working pressure of an LH_2 tank is 8.2 bar. Hence, the highest failing pressure is foreseen to be 32.8 bar_g. Therefore, a failing pressure of 34 bar was the upper limit adopted in the analysis to simulate the most severe consequences.

Table 8 collects the characteristics of the LH_2 storage tanks of the BMW and SH_2IFT tests considered in this analysis, while the initial conditions of the simulations are reported in Table 9.

Laboureur et al. (2014) provided a distinction to differentiate small-, mid- and large-scale tests in terms of TNT equivalent mass, that is $m_{TNT} > 1$ kg for large-scales, $m_{TNT} \approx 1$ kg for mid-scales, and $m_{TNT} < 1$ kg for small-scales. Therefore, the BMW experiments were small-scale tests while the SH_2IFT ones will be mid-scale. In addition, a cold BLEVE was provoked during the BMW tests, while a fired BLEVE will be initiated during the SH_2IFT tests. In this way, the proposed approach can be generalized since applied to two different test scales and BLEVE types. However, the experimental outcomes are required to validate the models and the approach, and establish if their generalization and predictive capabilities are successful.

4. Results

A graphical representation of the SCT model is depicted in Fig. 2 (a) where the dashed line is the tangent to the saturation curve at the critical point (CP), while in Fig. 2 (b), the p-h diagram for parahydrogen obtained after the application of the EB model is displayed.

In Table 10, the values of T_{SL} estimated for parahydrogen by the methods described in Sec. 3 are collected together with the correspondent pressures at saturation conditions. As shown, a BLEVE might occur after the catastrophic rupture of a LH_2 tank if the contained liquid has a temperature higher than 26.2 K, according to the most conservative method. The pressure correspondent to this temperature at saturation conditions is 4.2 bar.

Finally, Nishigaki and Saji (1983) identified experimentally the superheat temperature of oxygen, nitrogen, neon and hydrogen. The highest measured temperature for hydrogen at 1 atm was 28.1 K. This value is included in the range of temperatures theoretically estimated in this study. However, it is not clear if the hydrogen tested by Nishigaki and Saji (1983) had been converted in parahydrogen. There might be a small difference between the T_{SL} of parahydrogen and normal hydrogen since their critical temperatures slightly differ (NIST, 2019). The first method applied in this work, proposed by Reid (1976), seems the most accurate when compared with the experimental results.

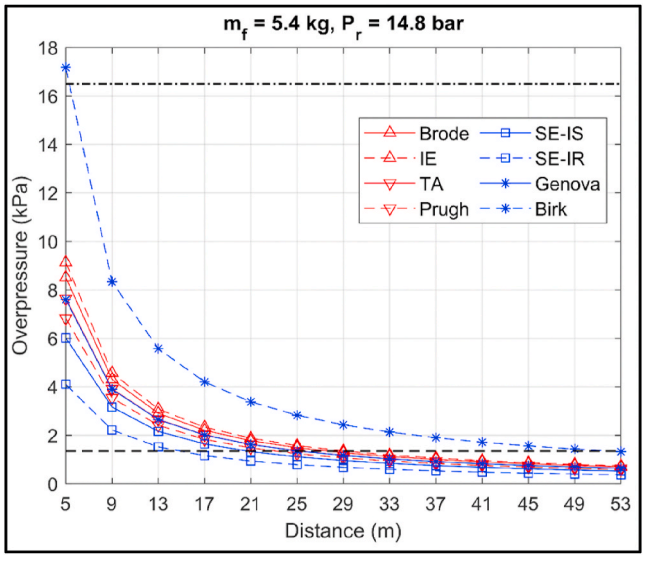

Fig. 5. Overpressure from the supercritical BLEVE blast wave at different distances from a tank failing at 14.8 bar and containing 5.4 kg of LH_2. Black dash-dotted and dashed lines indicate the overpressure thresholds at 16.5 and 1.35 kPa, respectively.

4.1. BMW safety test simulations

In the following, the consequence analysis results of the BMW safety tests are reported. Firstly, the mechanical energies estimated by the ideal and gas behaviour models for both sub- and supercritical BLEVEs are introduced. Secondly, the overpressures and impulses of the blast wave are presented. Finally, the fragments range and the fireball characteristics are described.

4.1.1. Mechanical energy

The mechanical energy generated from the failure at different pressures of the tanks filled with different amounts of LH_2 (1.8 and 5.4 kg) are displayed in Fig. 3.

Both sub- and supercritical BLEVEs were simulated by means of the models previously described. The mechanical energy was not estimated close to the critical point because the selected models cannot provide reliable results. For instance, the Genova model is influenced by the specific heat of the substance which tends towards an infinite value at the critical pressure. Among the chosen models, this is the only one that foresees a reduction of mechanical energy when the failure pressure increases at supercritical conditions, because it follows the trend of the hydrogen specific heat. Increasing the hydrogen mass inside the tank, the ideal gas behaviour models tend to ebb in the vicinity of the critical pressure at subcritical conditions. It should be noticed that the Birk model estimates higher mechanical energy values when the LH_2 mass inside the tank is lower at subcritical conditions, because it barely depends on the vapour phase. As previously mentioned, the TNO and Planas models cannot be employed at supercritical conditions. The most conservative model is the isothermal expansion (Smith and Van Ness, 1996), as already demonstrated in previously studies (Hemmatian et al., 2017b).

4.1.2. Overpressure and impulse from the blast wave

During the BMW safety tests (Pehr, 1996), the overpressure was measured at 3 m from the vessel, and the bursting pressures of the tanks were in the range from 2.0 to 14.8 bar. The subcritical and supercritical blast wave overpressures were then estimated by the ideal and real gas behaviour models at this distance from the tank in order to compare the experimental results (see Fig. 4). The failure pressure range was selected between 2.0 and 16.0 bar. It must be noticed that according to the results achieved in Sec. 3.1, the explosion which arise after the catastrophic rupture of the vessel can be considered as a BLEVE if the tank pressure before the explosion is higher than 4.2 bar. However, all the outcomes of the BMW tests were employed as comparison with the results of the selected models due to the scarcity in literature of small- and mid-scales LH_2 explosion experiments.

The most conservative estimation at subcritical conditions is provided by the TNO model with a maximum overpressure of 32 kPa at 11.25 bar. However, two BMW tests registered even a higher overpressure at 2 and 11 bar (16.7 and 47.0 kPa respectively). Pehr (1996) stated that during these two tests an over-proportional increase in overpressure was measured. The author supposed that the causes of these values can be attributed in one case to the overlap of the cutting charge and BLEVE effects (expanding of both vapour and liquid), and in the other case to an oxygen enrichment on the tank external wall due to an insulation damage. The highest overpressure (38.2 kPa) is attained by the Birk model at supercritical conditions when the tank fails at 16 bar and contains 5.4 kg of LH_2. For this reason, only the overpressures

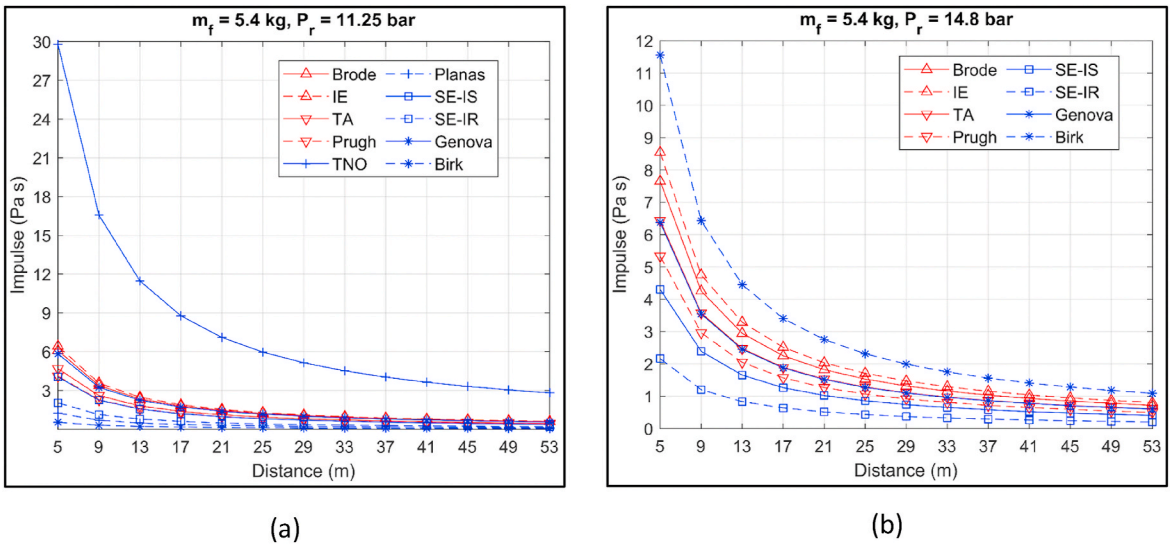

Fig. 6. Impulse from sub- and supercritical BLEVE blast waves at different distances from a tank containing 5.4 kg of LH_2 and failing at (a) 11.25 and (b) 14.8 bar, respectively.

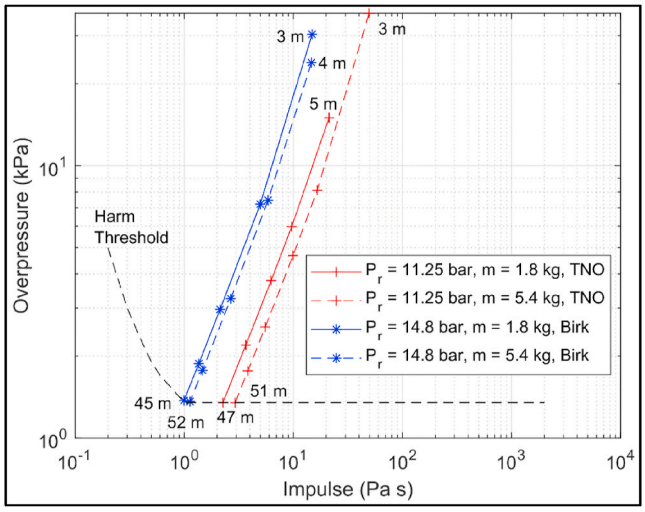

Fig. 7. Impulse and overpressure of both sub- and supercritical BLEVE blast waves at different distances from a tank failing at 11.25 and 14.8 bar respectively, containing 1.8 kg and 5.4 kg of LH_2, estimated with the most conservative models: TNO (red) and Birk (blue). The black dashed line indicates the harm threshold. (For interpretation of the references to colour in this figure legend, the reader is referred to the Web version of this article.)

Table 11
Fragments range for the sub- and supercritical BLEVEs occurred during the BMW safety tests estimated with the method proposed by (CCPS, 2010).

BLEVE types	Conditions at the explosion				*R* (and *H*) ranges (m)		
	m_{H2} (kg)	P_{rup} (bar)	E_k (kJ)	v_i (m s^{-1})	α_i = 5°	α_i = 10°	α_i = 45°
Subcritical BLEVE	5.4	11.25	14	21.6	8 (2)	16 (4)	48 (17)
Supercritical BLEVE	5.4	14.80	19	25.2	11 (3)	22 (6)	65 (23)

estimated at different distances when the rupture pressure is 14.8 bar (highest rupture pressure of the BMW tests) and the LH_2 mass is 5.4 kg are depicted in Fig. 5.

The overpressure thresholds of 16.5 and 1.35 kPa described in the methodology are represented by the dash-dotted and dashed lines in Fig. 5, respectively. In this case, if only the overpressure is considered, the 1.35 kPa threshold is attained at 52 m according to the most conservative model (Birk).

Differently from the overpressure, the highest impulse is estimated by the TNO model at subcritical conditions. For this reason, the impulses calculated at different distances from the LH_2 tank for both sub- and supercritical BLEVEs are displayed in Fig. 6.

As previously mentioned, the TNO model gives the highest estimation at subcritical conditions (29.8 Pa s at 5 m from the vessel), while the Birk model is the most conservative at supercritical conditions (11.6 Pa s at 5 m). The combined effect of overpressure and impulse is displayed in Fig. 7 where the most conservative estimations for both sub- and supercritical BLEVEs are reported. The safety distance from the tank to avoid undesired injuries is determined when the lines cross the harm threshold curve. The longest safety distance is 52 m and was achieved for the supercritical BLEVE when the tank fails at 14.8 bar and contains 5.4 kg.

4.1.3. *Fragments range*

The number of fragments of a cylindrical vessel after a BLEVE should be between two and three pieces (van den Bosch and Weterings, 2005). During the BMW tests, the cylindrical vessels fragmented in several pieces. The cut explosive charges employed to trigger the explosion could be responsible for the high number of vessel debris. The distance reached by the fragments during these tests was longer than 15 m (Pehr, 1996). The first method to determine the fragments range proposed by Birk (1996) for vessels with a volume lower than 5 m^3, provides an extremely conservative value of 157 m. The fragments ranges were estimated for both sub- and supercritical BLEVEs with the NFF method which neglect the fluid dynamic forces. For the subcritical explosion, the most conservative result ($\alpha_i = 45°$) was 47.6 and 64.7 m for the failure pressures of 11.25 and 14.8 bar respectively. As suggested by CCPS (2010), the initial angle of the fragments trajectory for a cylindrical vessel horizontally placed should be between 5° and 10°. The results obtained for $\alpha_i = 10°$ agree with the BMW test results (>15 m). The horizontal (*R*) and vertical (*H*) fragments ranges are collected in Table 11 together with the conditions prior the explosion.

Finally, the fragments range was estimated considering the fluid dynamic forces (CFF model). As previously mentioned, it was assumed that the tank ruptured in two main fragments, the end caps which have a hemispherical shape. The vessel diameter and the fragments mass are

Table 12
Fragments range for the sub- and supercritical BLEVEs occurred during the BMW safety tests estimated by including the fluid dynamic forces.

BLEVE types	Conditions at the explosion			Fragments characteristics			R (m)
	m_{H2} (kg)	P_{rup} (bar)	v_i (m s^{-1})	m_f (kg)	$C_D \cdot A_D$	$\frac{C_L \cdot A_L}{C_D \cdot A_D}$	
Subcritical BLEVE	5.4	11.25	21.6	30	0.077	0	47
Supercritical BLEVE	5.4	14.80	25.2	30	0.077	0	63

Table 13
Consequences of the fireballs occurred during the BMW safety tests.

Fireball parameters and safety distance	BMW test results	Consequence analysis	Relative error (%)
Max. diameter (m)	20	13.9	43.9
Height (m)	20	13.9	43.9
Duration (s)	4.0	0.8 ÷ 3.4	17.6 ÷ 400
Surface Emissive Power (kW m^{-2})	–	1880	–
Safety distance (therm. dose = 80 (kW m^{-2})$^{4/3}$ s)	–	77.8	–

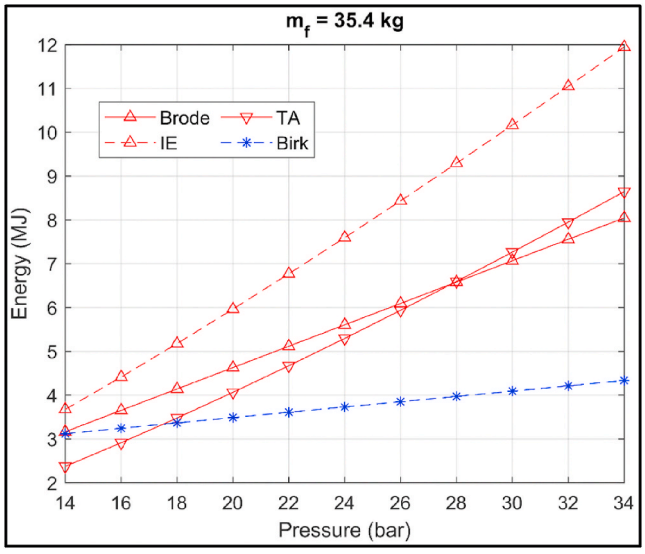

Fig. 8. Mechanical energy generated by supercritical BLEVE explosions at different tank pressures of a 1 m^3 tank containing 35.4 kg of LH_2, estimated by ideal (red) and real (blue) gas behaviour models. (For interpretation of the references to colour in this figure legend, the reader is referred to the Web version of this article.)

supposed to be 0.4 m and 30 kg respectively (the total tank mass is 60 kg). The results of the CFF method applied to the two BLEVE types are reported in Table 12, together with the fragments characteristics.

It must be noticed that similar ranges were obtained by the CFF and NFF models when an initial fragment angle of 45° was selected. These values are the most conservative results and can be assumed as upper limits, excluding the results achieved with the first method.

4.1.4. Fireball dimensions and radiation

The fireball consequences, that is its dimensions, duration, radiation and distance to the thermal dose threshold, are listed in Table 13. The results obtained in this study seem underestimating the fireball consequences when compared with the BMW safety tests. In particular, the maximum fireball diameter and height of 20 m was measured in the experiments, while 13.9 m was the highest values achieved from the empirical model, which are 30.5% lower. These estimations provide almost 44% of relative error. The fireball duration calculated with the buoyancy-dominated fireball formula was closer to the measured duration compared with the value obtained with the momentum-dominated equation, while according to the literature it should be the opposite. The *SEP* estimated theoretically with the Stefan-Boltzmann's law was more than five time higher compared to the maximum value suggested for the propane fireballs (350 kW m^{-2}). However, the model developed by Bader et al. (1971) for rocket liquid-propellants estimated a peak heat flux from the fireball of 4543 kW m^{-2} (400 Btu ft^{-2} s^{-1}). A similar result was estimated by Kite et al. (1965) during the Atlas/-Centaur abort (425 Btu ft^{-2} s^{-1}). In those analysis, large amounts of propellants were involved in the fireball, from 11,340 to 131,088 kg of both fuel and oxidizer, but the peak heat flux was not affected by the propellant mass. Considering the fireball duration and incident radiation, the thermal dose threshold of 80 (kW m^{-2})$^{4/3}$ s was estimated at 77.8 m from the centre of the exploding tank.

4.1.5. Safety distance

In this work, the safety distance is determined from the consequence analysis results. The highest value between the distance where the overpressure and impulse thresholds to avoid injuries are attained (52 m), the longest horizontal fragments range (65 m), the fireball diameter (13.9 m) and the distance to obtain the lowest thermal dose emitted from the fireball to the target (77.8 m), is considered as the safety distance. Therefore, it can be concluded that the safety distance from the vessel should be 77.8 m, due to the fireball radiation.

4.2. Models validation

The consequence analysis applied to the BMW safety tests, demonstrated that the most conservative models to estimate the overpressure from the blast wave in the sub- and supercritical conditions are the TNO and Birk ones, respectively. Furthermore, few models were able to provide higher overpressure values than the experimental results, if the highest BMW test outcomes attained at 2 and 11 bar (16.7 and 47.0 kPa, respectively) are excluded. These models are the Brode and IE, beyond the TNO and Birk ones. An observation must be made regarding the considerable underestimation obtained with the Birk model at subcritical conditions when the tank has a high filling degree and the liquid phase is preponderant. Moreover, the TA model foresees an overpressure increment when the rupture pressure increases at supercritical conditions (Fig. 4 (b)) slightly higher than the Brode model. In addition, the estimated overpressure by the TA model at supercritical condition is close to the experimental outcome. For these reasons, this model was considered valid as well. Finally, the selected energy models were the TNO, Birk, Brode, IE and TA. It must be remembered that the TNO model can be applied only at subcritical conditions. Laboureur et al. (2012b) simulated different small-scale supercritical propane BLEVE experiments by means of the models considered in this study. The comparison between the experimental and the estimated results demonstrated that the Birk and Prugh models provided the most conservative outcomes and were the only approaches that did not underestimated the measured overpressure.

Regarding the fragments range analysis, all three applied methods provided conservative results. However, the fragment range seems largely overestimated by the first method (157 m). For this reason, this model was not considered any further. On the other hand, the initial angle of the fragment must be chosen carefully when the NFF method is adopted, since the results obtained for angles lower than 10°

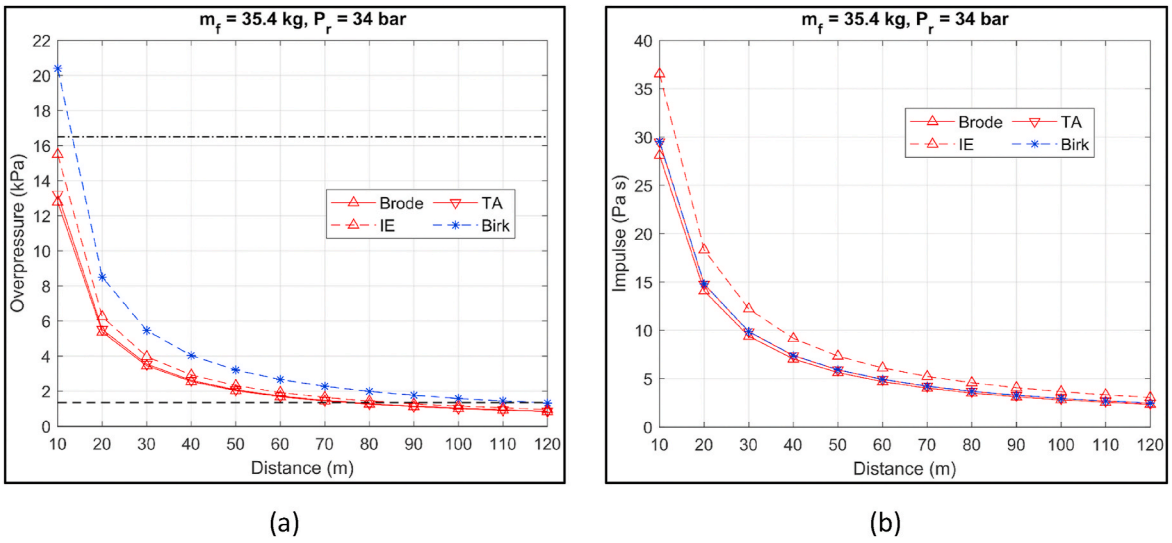

Fig. 9. (a) overpressure and (b) impulse at different distances from the blast wave of a supercritical BLEVE of a 1 m^3 tank containing 35.4 kg LH_2 and failing at 34.0 bar. The black dash-dotted and dashed lines represent the overpressure thresholds to avoid injuries.

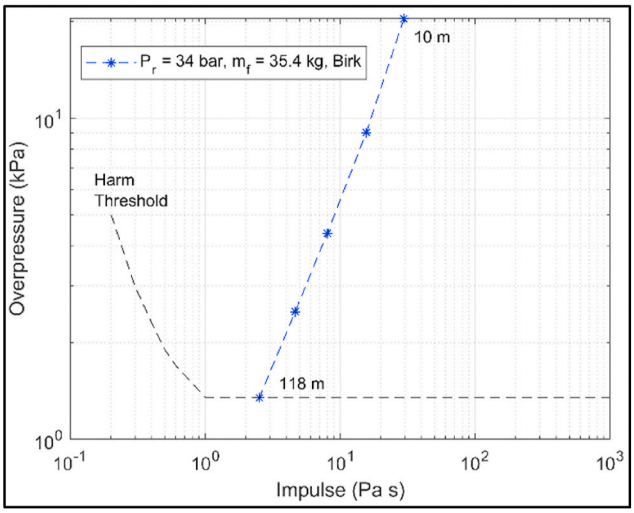

Fig. 10. Impulse and overpressure of the supercritical BLEVE blast wave at different distances from a tank failing at 34 bar and containing 35.4 kg of LH_2, estimated with the most conservative model (Birk). The black dashed line indicates the harm threshold.

Table 14
Fragments range for the supercritical BLEVE of the LH_2 tanks that will be tested during the SH_2IFT project, estimated by neglecting the fluid dynamic forces.

Tank insulation and mass	Conditions at the explosion				*R* (and *H*) ranges (m)		
	m_{H2} (kg)	P_{rup} (bar)	v_i (m s^{-1})	E_k (kJ)	α_i = 5°	α_i = 10°	α_i = 45°
MLI 730 kg	35.4	34.0	36.2	478	23 (6)	46 (12)	133 (47)
Perlite 1015 kg	35.4	34.0	30.7	478	17 (4)	33 (8)	96 (34)

underestimated the experimental results. Finally, the CFF model provided outcomes similar to the most conservative results attained by the second method with an initial fragment angle equal to 45°. Therefore, only the NFF and CFF models were considered valid and employed in the blind prediction study.

Table 15
Fragments range for the supercritical BLEVEs of the LH_2 tanks that will be tested during the SH_2IFT project, estimated by including the fluid dynamic forces.

Tank insulation and mass	Conditions at the explosion			Fragments characteristics			*R* (m)
	m_{H2} (kg)	P_{rup} (bar)	v_i (m s^{-1})	m_f (kg)	$C_D \cdot A_D$	$\frac{C_L \cdot A_L}{C_D \cdot A_D}$	
MLI 730 kg	35.4	34.0	36.2	365	0.88	0	135
Perlite 1015 kg	35.4	34.0	30.7	508	0.88	0	94

Table 16
Consequences of the fireballs expected during the SH_2IFT LH_2 BLEVE tests.

Fireball parameters and safety distance	Blind prediction
Max. diameter (m)	25.9
Height (m)	25.9
Duration (s)	1.5 ÷ 4.7
Surface Emissive Power (kW m^{-2})	1880
Safety distance (therm. dose = 80 (kW m^{-2})$^{4/3}$ s)	159.1

4.3. SH_2IFT project blind prediction study

The results of the blind prediction of the SH_2IFT project BLEVE tests are presented in this section with the same order of the previous section, starting from the mechanical energy generated by the explosion and related overpressure and impulse of the pressure wave and concluding with the fragments and fireball analysis.

4.3.1. Mechanical energy

The mechanical energy was calculated when the 1 m^3 tank filled with 35.4 kg of LH_2 fails in a tank pressure range comprise between 14 and 34 bar. Thus, only the supercritical conditions were considered in this blind prediction study since the most severe consequences are sought. The mechanical energy results are displayed in Fig. 8.

The isothermal expansion model is the most conservative model in this case, as well as for the BMW safety tests analysis. Again, all the models linearly increase with the rise in internal tank pressure.

4.3.2. Overpressure and impulse from the blast wave

Only the worst-case scenario was considered for the blind prediction

of the SH_2IFT LH_2 BLEVE tests. As previously mentioned, the maximum estimated failing pressure was 32.8 bar_g. Therefore, the overpressures and impulses were estimated at different distances from the vessel failing at 34 bar. In Fig. 9, both overpressures and impulses of the worst-case scenario are depicted.

The most severe overpressure estimations are achieved again by the Birk model, while the most conservative model to determine the impulse is the isothermal expansion. It must be noticed, that the ideal gas behaviour methods are not affected by the amount of fuel inside the tank at supercritical conditions, because the volume considered in the model equations corresponds to the total tank volume which is a fixed value. In Fig. 10, the plot of both overpressure and impulse against the harm threshold are depicted. In this case, the safety distance is attained at 118 m from the tank by the Birk model.

Ustolin et al. (2019) simulated with the aid of the Process hazard analysis software (PHAST) the overpressure from a BLEVE at different initial conditions for a tank with 1 m^3 volume and filled with different masses of LH_2. The authors obtained an overpressure of 2.07 kPa at 49.3 m when the tank pressure prior the explosion was 31.2 bar and 40 kg of LH_2 were contained in the vessel. Applying these conditions to the methodology selected in this study, this overpressure value is obtained at 47.5 and 75.1 m by the least (Brode) and the most (Birk) conservative models selected for this blind prediction study.

4.3.3. Fragments range

As result from the validation process, only the second and third fragments range models were implemented for the LH_2 vessels which will be tested during the SH_2IFT project. As for the blast wave, the fragment range was calculated only for the supercritical BLEVE of the two LH_2 tank types (with MLI and perlite insulation) failing at 34 bar, with the second method. As expected, the most conservative results were achieved by the NFF model when the initial fragments angle was 45°. The horizontal ranges were 133 and 96 m for the tanks with MLI and perlite insulations, respectively. The results are reported in Table 14.

Similarly, to the fragment analysis conducted for the BMW vessels, two main fragments (the end caps) are expected after a supercritical BLEVE of the LH_2 cylindrical tanks. Again, the ranges estimated by the CFF method, are close to the most conservative estimations obtained with the previous model. The ranges calculated with the last method are collected in Table 15 together with the fragments characteristics.

As previously mentioned, one tank will be installed in a vertical position during these tests. The vessel orientation may have an influence on the initial fragment angle. Moreover, if the tank has a substantial height some fragments can reach longer distances by starting their trajectory many meters above the ground compared with a tank placed horizontally. For these reasons, the most conservative estimation ($\alpha_i = 45°$) seems more likely for the vessel installed vertically.

4.3.4. Fireball dimensions and radiation

The maximum expected fireball diameter and height are 25.9 m, while the longest duration is 4.7 s. The safety distance from the SH_2IFT vessels should be 159.1 m in order to avoid a thermal dose higher than 80 $(kW\ m^{-2})^{4/3}$ s. Considering the comparison previously conducted in Sec. 4.1.4, these results might underestimate the real fireball consequences. The fireball dimensions and duration of the blind prediction study are reported in Table 16.

4.3.5. Safety distance

In this case, the longest safety distance was 159.1 m due to the fireball radiation, compared with the distance to achieve the overpressure and impulse thresholds to avoid injuries (118 m), the fragments range (135 m), and the fireball diameter (25.4 m).

5. Discussion

The equations to calculate the mechanical energy of the explosion adopted in this study, provided a wide range of results, with a difference of one order of magnitude between the most and the least conservative models. In particular, the ideal gas behaviour models provided higher values compared with the real gas behaviour ones. The most conservative models were the isothermal expansion (Smith and Van Ness, 1996) and Brode (1959), as already ascertained by Hemmatian et al. (2017b), while the TNO approach (van den Bosch and Weterings, 2005) was the most conservative real gas behaviour model. Instead, the least conservative method was the one proposed by Genova et al. (2008). In general, if the vessel ruptures at subcritical conditions close to the critical pressure, all the models overpressure curves reach a plateau or have a decreasing trend, except the Genova and TNO methods. This trend can be noticed in Fig. 3 (b), especially for the ideal gas behaviour models. On the other hand, at supercritical conditions the employed models always have a rising trend except the Genova model which is affected by the specific heat at constant pressure (c_p) of the substance. Therefore, the Genova method seems not appropriate when applied to the BLEVE assessment for LH_2. As mentioned before, the models which take into account both the vapour and liquid phases (TNO and Planas (Planas-Cuchi et al., 2004)) cannot be applied at supercritical conditions. Instead, the models which depends on barely the vapour phase are more conservative when the tank has a low filling degree, and vice versa for the methods which are influenced only by liquid phase. This means that a significant error can be committed when the non-considered phase is dominant in the vessel (Hemmatian et al., 2017a). Moreover, the ideal behaviour models are not affected by the change in density (filling degree) at supercritical conditions because the entire volume of the tank and its pressure are the only two parameters considered by these methods.

The mechanical energy results are exploited in different manners to estimate the overpressure and impulse generated by the blast wave, and the fragments range. The ground reflection and tank geometry effects are included in the TNO and Birk methods to calculate the blast wave yield. For these reasons, the highest values of overpressure and impulse were obtained by these two approaches. On the contrary, according to the Planas, superheat energy (Casal and Salla, 2006) and Genova models, only a fraction of the mechanical energy contributes to the blast wave. This fraction depends on the tank fractur type (fragile, 80%, or ductile, 40%) for the Planas model, on the type of thermodynamic process (isentropic, 14%, or irreversible, 5%) for the SE model, and on empirical correlations (7% for propane) for the Genova method. In the case of double walled tank, used to contain cryogenic fluids such as LH_2, how will be affected this percentage? For instance, more energy should be spent to rupture the two tanks (inner and outer), or the outer vessel, designed to bear the vacuum pressure, does not influence the energy required for the fracture? These models (except the Genova one) were validated for butane and propane BLEVEs by Hemmatian et al. (2017b). However, they seem not accurate when applied to the LH_2 BLEVEs, even though the model outcomes were validated with the BMW safety tests results in which single walled LH_2 tanks were tested. As demonstration of this, the SE model provided the least conservative results for overpressures and impulses. Regarding the model validations with this set of results, only the outcomes of the TNO and Brode models had higher values than the experimental results at subcritical conditions, if the two tests with the over-proportional increase in overpressure are excluded. Since only one test was conducted at supercritical conditions, it is more crucial to conclude which are the most appropriate models at this thermodynamic status. However, the Birk (Birk et al., 2007), Brode, IE and TA (Crowl, 1992, 1991) models were the most conservative. In particular, the Birk method evaluated overpressure values which are more than 200% higher than the measured ones. Finally, it can be proposed to estimate the overpressure from the blast wave of an LH_2 BLEVE with the TNO model when the substance conditions are subcritical immediately prior the explosion, and with the Birk model for a supercritical BLEVE.

One observation regarding the TNT equivalent mass method

employed in this study must be made. In the case of BLEVE and high-pressure vessels, this method offers overly conservative estimations in the near field and conservative approximations in the far field due to the different energy release process of the high explosives (very fast) and the vessels explosion (slower than explosives) (Birk et al., 2007). The Sachs scaling law (Sachs, 1944), which derives always from experimental data on explosives, generally provides a less conservative estimation of the pressure wave effects. However, in this study, different underestimations were highlighted by the models previously discussed even adopting the most conservative method (TNT equivalent mass). It is true that in this analysis only the far field was considered due to the lack in experimental data, and more focus should be placed on the pressure wave effects in the near field in the future.

The results obtained for the blind prediction study of the mid-scale SH_2IFT tests cannot be compared since the only available tests in literature are the BMW ones, which are small scale experiments ($W_{TNT} < 1$ kg). It must be noticed that the distances at which the overpressure threshold to avoid any kind of injuries on humans was attained are 52 m in the worst-case scenario for the BMW tank containing 5.4 kg of LH_2 exploding at 14.8 bar, and 118 m for the SH_2IFT vessel containing 35.4 kg of LH_2 and failing at 34 bar. Thus, from one analysis to the other, the safety distance and the tank pressure increase almost 2.3 times, while the tank volume and LH_2 mass were almost 8.3 and 6.6 times larger. Further investigations and experiments are needed to comprehend which is the correlation between the vessel parameters to achieve a generalization of the approach. In this manner, the method can be applied to all the hydrogen accident scenarios in which BLEVE represents one of the consequences.

The estimation of the fragments range is critical for a BLEVE consequence analysis and is challenging due to several uncertainties. Firstly, the parameters which influence the range calculation such as the fragment shape, dimension, mass, and initial angle are unknown a priori. Secondly, the different methods provide quite contrasting results. For instance, the method proposed by Birk (1996) was the first one employed in this analysis and the most conservative. The results obtained with this approached were almost three times higher than the longest range foreseen by the other models, and thus was not employed in the blind prediction study. The NFF approach estimated quite different range by varying the fragment initial angle. In particular, the fragment range increased two times modifying the angle from 5° to 10°, and almost six times from 5° to 45° (most conservative case). In this case, the fluid dynamic forces were neglected, and this can lead to either an overestimation or an underestimation of the fragment range. This latter may be caused by the frisbee effect which manifests when disc-shape fragments are thrown with low initial angle (CCPS, 2010). In this case, high lift forces are generated under the debris, thus ensuing in an even longer range. However, the CFF approach selected in this study estimated similar range values to the most conservative estimation ($\alpha_i = 45°$) of the NFF model. The assumption of the last employed method (CFF) was that the tanks ruptures in two main pieces (the end caps) which have a hemispherical shape, therefore the frisbee effect was not considered.

Comparing the two case studies (BMW and SH_2IFT), it can be noticed that the fragment ranges do not vary linearly with the LH_2 mass contained in the tanks. In particular, the ranges increase from two to almost three times by using the first or the NFF and CFF methods, while the LH_2 mass increases five times and the maximum mechanical energy generated by the explosion is 24 times higher. The reason for this is that the equations of the models consider the mass of the empty vessels as well. In this regard, if this mass is lighter compared with a heavier vessel, as occurs for the MLI insulated tank, the range of the fragments may be longer when the same kinetic energy is produced by the explosion. Hence, the reduction of the vessel weight sought in many applications, such as the automotive one, would not aid the consequences mitigation of an eventual accident with subsequent explosion. Finally, the fragment range values obtained in this analysis seem extremely conservative when compared with the few LH_2 tank explosion accidents available in literature. The longest distance reached by the fragments after the S-IV all systems vehicle explosion was 457 m, and the LH_2 and LOX amounts were 7690 and 38,212 kg, respectively (Gayle, 1964). During the accident analysed by Mires (1985), the longest horizontal and vertical fragment ranges were 76 and 1.8 m for the 34 m^3 tank almost full with 2411 kg of LH_2. Another question arises regarding the influence of the vapour and liquid phases on the fragment range, since the container were filled mostly with hydrogen in liquid phase during the two considered accident scenarios ((Gayle, 1964) and (Mires, 1985)). Therefore, further investigations are needed also in this case, especially because the outcomes of this work indicated that the consequences provoked by the fragments are more severe than the ones caused by the pressure wave.

The consequences of the hydrogen fireball ignited after the explosion were estimated with the analytical models previously described and usually employed in risk analysis. These equations underestimated the fireball diameter and duration. It was not possible to validate the radiation emitted from the fireballs during the BMW safety tests because no data were reported in (Pehr, 1996). The radiation was calculated theoretically with the most conservative approach, i.e. the Stefan-Boltzmann's law. In fact, an extremely high value of *SEP* was obtained (1880 kW m^{-2}), more than five times higher than the theoretical *SEP* value of propane fireball. The reason for this value is the elevated temperature of the stochiometric combustion of hydrogen and air (2321 K (NASA, 2005)). Pehr (1996) assumed that the temperature of the burning gas inside the fireball reached this value during the BMW tests. From the incident radiation, the thermal dose threshold of 80 (kW m^{-2})$^{4/3}$ s was estimated at 77.8 and 159.1 m for the BMW and SH_2IFT tests, respectively. In (Shentsov et al., 2016), this thermal dose threshold was measured at 72.5 m for a compressed hydrogen tank containing 1.64 kg of hydrogen and failing at 35.7 MPa. This result seems to agree with the outcome of this study. However, further experimental results are needed to validate these analyses. Furthermore, different authors stated that the hydrogen fireballs generated in their experiments were quite luminous and the emitted radiation was largely different from the hydrogen jet fire. This was mentioned by Zalosh and Weyandt (2005), explaining that the propane fire which was burning beneath the vessel could have contribute to the fireball. Similar observation about the radiation were made by Pehr (1996), who reported the BMW tests results. As previously mentioned, cold BLEVEs were triggered during those tests, thus the authors explained that the radiation was provoked by the burning of solid particles in the air and insulating materials. Finally, High (1968) estimated through his empirical model, a radiation of 229.4 and 36.8 kW m^{-2} (20.2 and 3.24 Btu ft^{-2} s^{-1}), respectively at 610 and 1524 m (2000 and 5000 ft) from a fireball with a radius of 215 m and a duration of 33.9 s. The lowest value corresponds to a thermal dose of 4150 (kW m^{-2})$^{4/3}$ s, hence far from the 80 (kW m^{-2})$^{4/3}$ s threshold.

The assessment of the three main consequences was fundamental to comprehend which is the safety distance from the exploding tank. The blast wave effects do not strongly affect the safety distance. In fact, the overpressure and impulse threshold to avoid any kind of injuries was the shortest distance compared with the fragment range and the thermal dose threshold distance. This is confirmed by Planas and Casal (2016) who stated that fragments impact and thermal radiation from the fireball may have effects over a large area around the explosion, while the pressure wave usually do not reach distances far from the failing vessel. However, the blast wave can highly damage structures in the near field, therefore further experimental data are needed.

As previously mentioned, the tanks tested during the BMW experiments were single walled type, covered with a layer of foam as insulation. Therefore, the results obtained in these tests do not represent a realistic accident scenario, because double walled tanks are currently employed to store LH_2. The lack of experimental data lead to several uncertainties for the modelling activity of the BLEVE phenomenon. For instance, the fractions of mechanical energy responsible for the vessel

rupture, pressure wave generation, and fragments ejection, might be different from the traditional single walled propane tanks. Moreover, the propane tanks engulfed in fires usually fracture on the top immediately prior the BLEVE (Birk et al., 2007), because the specific heat of the vapour phase is lower than the liquid one, thus the heat absorbed by the tank wall is higher in the vapour region and the metal degrades faster. The parahydrogen specific heat at saturation conditions is slightly higher for the vapour rather than the liquid phase. This means that the vapour phase absorbs a larger amount if its mass is the same or heavier than the liquid one, i.e. when the tank filling degree is low. Therefore, additional studies are needed to understand the structural behaviour of the vessel as well.

Finally, the consequences of an LH_2 BLEVE estimated in this work should be thoroughly validated with further experimental results and then compared with the BLEVE consequences of other fuels. This comparison can be conducted in different manners due to the peculiar hydrogen properties. For instance, if the tank volume is adopted as reference, the parahydrogen mass would be much lower than the other fuels due to its density. On the other hand, if similar masses are compared, it would result in a considerable larger LH_2 tank volume. Probably the best fashion would be to compare the same tank energy content by taking into account the LHV of the different fuels. According to (Hansen, 2020), the consequences of an eventual LH_2 BLEVE should be less severe than an LNG tank explosion, but further data are required to confirm this assessment. From the results of the NASA projects about the rocket propellants explosions, Gayle (1964) concluded that the LOX/LH_2 consequences have a lower yield compare with the other propellants such as LOX/RP-1, but the probabilities for an accident to occur seem higher for the LH_2 due to its extreme flammability. Therefore, the probabilities should also be investigated in order to conduct an exhaustive risk analysis.

6. Conclusions

In this study, a thorough consequence analysis of LH_2 BLEVEs for both small- and mid-scale tests was conducted for the first time by evaluating all the consequence typologies (pressure wave, fragments, and fireball). The analytical and theoretical models usually employed in risk analysis were adopted, and an underestimation was observed when the outcomes were compared with the experimental results. The drawbacks of the models were highlighted together with different uncertainties such as the behaviour of the double walled tank and of LH_2 during the evolution of the BLEVE phenomenon. It can be concluded that a broad knowledge gap is still present regarding the LH_2 physical explosions.

The results of the different models were validated with the BMW safety tests outcomes, and the most appropriate methods were selected for the blind prediction study. The blind prediction case study addressed the planned SH_2IFT LH_2 BLEVE tests. The blind prediction results provided in this study must be validated by the experiments. This will further support the selection of the most appropriate consequence models and eventually serve as development of new approaches. Furthermore, effective safety barriers to prevent or mitigate the LH_2 BLEVE can be selected once the experimental results will be available. It is suggested to enhance the consequence analysis by employing innovative tools such as computational fluid dynamics (CFD) codes. Moreover, the finite elements method (FEM) can be adopted to conduct a suitable structural analysis of the double walled tank. Therefore, this analysis could be coupled with a CFD study to comprehend how the fluid inside the tank and the eventual external fire stress the tank material, by developing a Multiphysics simulation tool. Finally, a comparison between the consequences of the BLEVE for LH_2 and other conventional fuels (hydrocarbons) would be of high importance to aid the writing of safety codes and regulations. When the consequence analysis will be concluded, a probability analysis would be crucial in the case of hydrogen to provide a complete risk analysis overview.

Author statement

Federico Ustolin: Conceptualization, Methodology, Software, Validation, Writing - Original Draft. **Nicola Paltrinieri**: Methodology, Writing - Review and Editing, Supervision, Funding acquisition. **Gabriele Landucci**: Writing - Review and Editing, Supervision.

Declaration of competing interest

The authors declare that they have no known competing financial interests or personal relationships that could have appeared to influence the work reported in this paper.

Acknowledgments

This work was undertaken as part of the research project Safe Hydrogen fuel handling and Use for Efficient Implementation (SH_2IFT), and the authors would like to acknowledge the financial support of the Research Council of Norway under the ENERGIX programme (Grant No. 280964).

References

Bader, B.E., Donaldson, A.B., Hardee, H.C., 1971. Liquid-propellant rocket abort fire model. J. Spacecraft Rockets 8, 1216–1219.
Bagster, D.F., Pitblado, R.M., 1989. Thermal hazards in the process industry. Chem. Eng. Prog. 85, 69–75.
Baker, W.E., Cox, P.A., Kulesz, J.J., Strehlow, R.A., Westine, P.S., 1983. Explosion Hazards and Evaluation. Elsevier Science, New York.
Barron, R.F., Nellis, G.F., 2016. Cryogenic Heat Transfer, second ed. CRC Press, Boca Raton. http://dx.doi.org/10.1201/b20225.
Barthelemy, H., Weber, M., Barbier, F., 2017. Hydrogen storage: recent improvements and industrial perspectives. Int. J. Hydrogen Energy 42, 7254–7262. http://dx.doi.org/10.1016/J.IJHYDENE.2016.03.178.
Baum, M.R., 1984. The velocity of missiles generated by the disintegration of gas-pressurized vessels and pipes. J. Pressure Vessel Technol. 106, 362–368. http://dx.doi.org/10.1115/1.3264365.
Beyler, C., 2016. Fire hazard calculations for large, open hydrocarbon fires. In: Hurley, M. (Ed.), SFPE Handbook of Fire Protection Engineering. Springer Science + Business Media, LLC, New York, pp. 2591–2663. http://dx.doi.org/10.1007/978-1-4939-2565-0.
Birk, A.M., 1996. Hazards from propane BLEVEs: an update and proposal for emergency responders. J. Loss Prev. Process. Ind. 9, 173–181. http://dx.doi.org/10.1016/0950-4230(95)00046-1.
Birk, A.M., Davison, C., Cunningham, M., 2007. Blast overpressures from medium scale BLEVE tests. J. Loss Prev. Process. Ind. 20, 194–206. http://dx.doi.org/10.1016/J.JLP.2007.03.001.
Bracha, M., Lorenz, G., Patzelt, A., Wanner, M., 1994. Large-scale hydrogen liquefaction in Germany. Int. J. Hydrogen Energy 19, 53–59. http://dx.doi.org/10.1016/0360-3199(94)90177-5.
Brode, H.L., 1959. Blast wave from a spherical charge. Phys. Fluids 2, 217–229. http://dx.doi.org/10.1063/1.1705911.
Cardella, U., Decker, L., Sundberg, J., Klein, H., 2017. Process optimization for large-scale hydrogen liquefaction. Int. J. Hydrogen Energy 42, 12339–12354. http://dx.doi.org/10.1016/J.IJHYDENE.2017.03.167.
Casal, J., 2008. Evaluation of the Effects and Consequences of Major Accidents in Industrial Plants. Elsevier, Amsterdam.
Casal, J., Arnaldos, J., Montiel, H., Planas-Cuchi, E., Vilchez, J., 2001. Modelling and understanding BLEVEs. Handbook of Hazardous Materials Spills Technology. McGraw-Hill, New York.
Casal, J., Hemmatian, B., Planas, E., 2016. On BLEVE definition, the significance of superheat limit temperature (Tsl) and LNG BLEVE's. J. Loss Prev. Process. Ind. 40, 81. http://dx.doi.org/10.1016/j.jlp.2015.12.001.
Casal, J., Salla, J.M., 2006. Using liquid superheating energy for a quick estimation of overpressure in BLEVEs and similar explosions. J. Hazard Mater. 137, 1321–1327. http://dx.doi.org/10.1016/J.JHAZMAT.2006.05.001.
Ccps, 2010. Guidelines for Vapor Cloud Explosion, Pressure Vessel Burst, BLEVE, and Flash Fire Hazards, second ed. Wiley Subscription Services, Inc., A. Wiley Company, New York. http://dx.doi.org/10.1002/9780470640449.
Crowl, D.A., 1992. Calculating the energy of explosion using thermodynamic availability. J. Loss Prev. Process. Ind. 5, 109–118. http://dx.doi.org/10.1016/0950-4230(92)80007-U.
Crowl, D.A., 1991. Using thermodynamic availability to determine the energy of explosion. Plant/Operations Prog. 10, 136–142.
D'Ovidio, G., Ometto, A., Valentini, O., 2020. A novel predictive power flow control strategy for hydrogen city rail train. Int. J. Hydrogen Energy 45, 4922–4931. http://dx.doi.org/10.1016/j.ijhydene.2019.12.067.

Fumey, B., Buetler, T., Vogt, U.F., 2018. Ultra-low NOx emissions from catalytic hydrogen combustion. Appl. Energy 213, 334–342. http://dx.doi.org/10.1016/J.APENERGY.2018.01.042.
Gayle, J.B., 1964. Investigation of S-IV All Systems Vehicle Explosion, vol. 563. NASA TN D.
Gayle, J.B., Bransford, J.W., 1965. Size and Duration of Fireballs from Propellant Explosions - NASA TM X-53314.
Genova, B., Silvestrini, M., Leon Trujillo, F.J., 2008. Evaluation of the blast-wave overpressure and fragments initial velocity for a BLEVE event via empirical correlations derived by a simplified model of released energy. J. Loss Prev. Process. Ind. 21, 110–117. http://dx.doi.org/10.1016/J.JLP.2007.11.004.
Hansen, O.R., 2020. Liquid hydrogen releases show dense gas behavior. Int. J. Hydrogen Energy 45, 1343–1358. http://dx.doi.org/10.1016/j.ijhydene.2019.09.060.
Hemmatian, B., Casal, J., Planas, E., 2017a. A new procedure to estimate BLEVE overpressure. Process Saf. Environ. Protect. 111, 320–325. http://dx.doi.org/10.1016/J.PSEP.2017.07.016.
Hemmatian, B., Planas, E., Casal, J., 2017b. Comparative analysis of BLEVE mechanical energy and overpressure modelling. Process Saf. Environ. Protect. 106, 138–149. http://dx.doi.org/10.1016/j.psep.2017.01.007.
High, R.W., 1968. The Saturn fireball. Ann. N. Y. Acad. Sci. 152, 441–451. http://dx.doi.org/10.1111/j.1749-6632.1968.tb11992.x.
Hord, J., 1972. Explosion Criteria for Liquid Hydrogen Test Facilities. NBS Report.
HydrogenTools, 2017. Liquid hydrogen tank boiling liquid expanding vapor explosion (BLEVE) due to water-plugged vent stack [WWW Document]. URL. https://h2tools.org/lessons/liquid-hydrogen-tank-boiling-liquid-expanding-vapor-explosion-bleve-due-water-plugged-vent. (Accessed 6 March 2020).
IEA, 2019. The Future of Hydrogen - Seizing Today's Opportunities.
Johnson, D.M., Pritchard, J.M., Wickens, M.J., 1991. Large scale experimental study of boiling liquid expanding vapour explosions (BLEVEs). Contract report 15367, project M8411. Research and Technology division, British Gas.
Jovanović, A.S., Baloš, D., 2013. INTeg-Risk project: concept and first results. J. Risk Res. 16, 275–291. http://dx.doi.org/10.1080/13669877.2012.729516.
Kinney, G., Graham, K., 1985. Explosive Shocks in Air. Springer, New York.
Kite, F.D., Webb, D.M., Bader, B.E., 1965. Launch Hazards Assessment Program, Report on Atlas/Centaur Abort - SC-RR, pp. 65–333.
Laboureur, D., 2012. Experimental Characterization and Modeling of Hazards: BLEVE and Boilover (PhD Dissertation). Von Karman Institute for Fluid Dynamics (Universite Libre de Bruxelles).
Laboureur, D., Buchlin, J.M., Rambaud, P., 2012a. Small scale experiments on boiling liquid expanding vapor explosions: supercritical BLEVE. ASME 2012 Pressure Vessels and Piping Conference, pp. 51–60. http://dx.doi.org/10.1115/PVP2012-78283.
Laboureur, D., Heymes, F., Aprin, L., Buchlin, J.M., Rambaud, P., 2012b. BLEVE overpressure: small scale experiments and multi-scale comparison with literature survey of blast wave modeling. Global Congress on Process Safety.
Laboureur, D., Heymes, F., Lapebie, E., Buchlin, J., Rambauda, P., 2014. BLEVE overpressure: multiscale comparison of blast wave modeling. Process Saf. Prog. 33, 274–284. http://dx.doi.org/10.1002/prs.11626.
Landucci, G., Tugnoli, A., Cozzani, V., 2010. Safety assessment of envisaged systems for automotive hydrogen supply and utilization. Int. J. Hydrogen Energy 35, 1493–1505. http://dx.doi.org/10.1016/j.ijhydene.2009.11.097.
Lowesmith, B.J., Hankinson, G., Chynoweth, S., 2013. Safety issues of the liquefaction, storage and transportation of liquid hydrogen: studies in the IDEALHY project. In: International Conference on Hydrogen Safety. Brussels, Belgium.
Maggio, G., Nicita, A., Squadrito, G., 2019. How the hydrogen production from RES could change energy and fuel markets: a review of recent literature. Int. J. Hydrogen Energy 44, 11371–11384. http://dx.doi.org/10.1016/j.ijhydene.2019.03.121.
McAllister, S., Chen, J.-Y., Fernandez-Pello, A.C., 2011. Fundamentals of Combustion Processes. Springer Science +Business Media, LLC, New York. http://dx.doi.org/10.1007/978-1-4419-7943-8.
Mires, R.W., 1985. Analysis of liquid hydrogen explosion. Phys. Teach. 23, 533–535. http://dx.doi.org/10.1119/1.2341906.
Molkov, V., Kashkarov, S., 2015. Blast wave from a high-pressure gas tank rupture in a fire: stand-alone and under-vehicle hydrogen tanks. Int. J. Hydrogen Energy 40, 12581–12603. http://dx.doi.org/10.1016/J.IJHYDENE.2015.07.001.
NASA, 2020. Air properties definitions [WWW Document]. URL. https://www.grc.nasa.gov/www/k-12/BGP/airprop.html. (Accessed 27 May 2020).
NASA, 2005. Safety standard for hydrogen and hydrogen systems, guidelines for hydrogen system design, materials selection, operations, storage, and transportation. NSS 1740, 16.
NASA, 1997. Report of the presidential commission on the space shuttle challenger accident (1986) [WWW Document]. URL. http://science.ksc.nasa.gov/shuttle/missions/51-l/docs/rogers-commission/table-ofcontents.html. (Accessed 11 June 2019).
NCE Maritime Cleantech, 2019. Norwegian Future Value Chains for Liquid Hydrogen.
Nishigaki, K., Saji, Y., 1983. On the limit of superheat of cryogenic liquids. Cryogenics 23, 473–476. http://dx.doi.org/10.1016/0011-2275(83)90004-8.
NIST, 2019. NIST Chemistry WebBook [WWW Document]. URL. webbook.nist.gov/. (Accessed 19 March 2019).
Notardonato, W.U., Swanger, A.M., Fesmire, J.E., Jumper, K.M., Johnson, W.L., Tomsik, T.M., 2017. Zero Boil-Off Methods for Large Scale Liquid Hydrogen Tanks Using Integrated Refrigeration and Storage. NASA Technical Reports Server (NTRS). http://dx.doi.org/10.1088/1757-899X/278/1/012012.
Ono, R., Nifuku, M., Fujiwara, S., Horiguchi, S., Oda, T., 2007. Minimum ignition energy of hydrogen–air mixture: effects of humidity and spark duration. J. Electrost. 65, 87–93. http://dx.doi.org/10.1016/J.ELSTAT.2006.07.004.
Paltrinieri, N., Landucci, G., Molag, M., Bonvicini, S., Spadoni, G., Cozzani, V., 2009. Risk reduction in road and rail LPG transportation by passive fire protection. J. Hazard Mater. 167, 332–344. http://dx.doi.org/10.1016/j.jhazmat.2008.12.122.
Paltrinieri, N., Øien, K., Cozzani, V., 2012. Assessment and comparison of two early warning indicator methods in the perspective of prevention of atypical accident scenarios. Reliab. Eng. Syst. Saf. 108, 21–31. http://dx.doi.org/10.1016/j.ress.2012.06.017.
Pehr, K., 1996. Aspects of safety and acceptance of LH2 tank systems in passenger cars. Int. J. Hydrogen Energy 21, 387–395. http://dx.doi.org/10.1016/0360-3199(95)00092-5.
Peschka, W., 1992. Liquid Hydrogen - Fuel of the Future, first ed. Springer-Verlag, Wien. http://dx.doi.org/10.1007/978-3-7091-9126-2.
Planas-Cuchi, E., Salla, J.M., Casal, J., 2004. Calculating overpressure from BLEVE explosions. J. Loss Prev. Process. Ind. 17, 431–436. http://dx.doi.org/10.1016/J.JLP.2004.08.002.
Planas, E., Casal, J., 2016. BLEVE-Fireball. In: Lackner, M., Winter, F., Agarwal, A.K. (Eds.), Handbook of Combustion. Wiley-VCH Verlag GmbH & Co. KGaA, Weinheim. http://dx.doi.org/10.1002/9783527628148.hoc093.
Prugh, R.W., 1994. Quantitative evaluation of fireball hazards. Process Saf. Prog. 13, 83–91. http://dx.doi.org/10.1002/prs.680130211.
Prugh, R.W., 1991. Quantitative evaluation of "BLEVE" hazards. J. Fire Protect. Eng. 3, 9–24.
Reid, R., 1979. Possible mechanism for pressurized-liquid tank explosions or BLEVE's. Science 203 (80), 1263–1265. http://dx.doi.org/10.1126/science.203.4386.1263.
Reid, R., 1976. Superheated liquids. Am. Sci. 64, 146–156.
Rew, P.J., 1997. LD50 Equivalent for the Effect of Thermal Radiation on Humans - CRR 129/1997.
Rybin, H., Krainz, G., Bartlok, G., Kratzer, E., 2005. Safety demands for automotive hydrogen storage systems. International Conference on Hydrogen Safety.
Sachs, R.G., 1944. The Dependence of Blast on Ambient Pressure and Temperature, BRL Report No. 466. Aberdeen Proving Ground, Maryland.
Salla, J.M., Demichela, M., Casal, J., 2006. BLEVE: a new approach to the superheat limit temperature. J. Loss Prev. Process. Ind. 19, 690–700. http://dx.doi.org/10.1016/j.jlp.2006.04.004.
Shentsov, V., Cirrone, D.M.C., Makarov, D., Molkov, V., 2016. Simulation of fireball and blast wave from a hydrogen tank rupture in a fire. In: 7th International Symposium on Non-equilibrium Processes, Plasma, Combustion, and Atmospheric Phenomena, Sochi, Russia, pp. 139–146.
Skjold, T., Hisken, H., Bernard, L., Mauri, L., Atanga, G., Lakshmipathy, S., Lucas, M., Carcassi, M., Schiavetti, M., Chandra Madhav Rao, V., Sinha, A., Wen, J.X., Tolias, I. C., Giannissi, S.G., Venetsanos, A.G., Stewart, J.R., Hansen, O.R., Kumar, C., Krumenacker, L., Laviron, F., Jambut, R., Huser, A., 2019. Blind-prediction: estimating the consequences of vented hydrogen deflagrations for inhomogeneous mixtures in 20-foot ISO containers. J. Loss Prev. Process. Ind. 61, 220–236. http://dx.doi.org/10.1016/j.jlp.2019.06.013.
Smith, J.M., Van Ness, H.C., 1996. Introduction to Chemical Engineering Thermodynamics, fifth ed. McGraw-Hill, Inc, NewYork.
Stochl, R.J., Knoll, R.H., 1991. Thermal Performance of a Liquid Hydrogen Tank Multilayer Insulation System at Warm Boundary Temperatures of 630, 530 and 152 °R - NASA TM 104476.
Trevisani, L., Fabbri, M., Negrini, F., Ribani, P.L., 2007. Advanced energy recovery systems from liquid hydrogen. Energy Convers. Manag. 48, 146–154. http://dx.doi.org/10.1016/j.enconman.2006.05.002.
Ullah, A., Ahmad, F., Jang, H.-W., Kim, S.-W., Hong, J.-W., 2017. Review of analytical and empirical estimations for incident blast pressure. KSCE J. Civ. Eng. 21, 2211–2225. http://dx.doi.org/10.1007/s12205-016-1386-4.
Ustolin, F., Paltrinieri, N., 2020. Hydrogen fireball consequence analysis. Chem. Eng. Trans. 82, 211–216. http://dx.doi.org/10.3303/CET2082036.
Ustolin, F., Paltrinieri, N., Berto, F., 2020. Loss of integrity of hydrogen technologies: a critical review. Int. J. Hydrogen Energy 45, 23809–23840. http://dx.doi.org/10.1016/j.ijhydene.2020.06.021.
Ustolin, F., Song, G., Paltrinieri, N., 2019. The influence of H2 safety research on relevant risk assessment. Chem. Eng. Trans. 74 http://dx.doi.org/10.3303/CET1974233.
van Biert, L., Godjevac, M., Visser, K., Aravind, P.V., 2016. A review of fuel cell systems for maritime applications. J. Power Sources 327, 345–364. http://dx.doi.org/10.1016/J.JPOWSOUR.2016.07.007.
van den Bosch, C.J.H., Weterings, R.A.P.M., 2005. Methods for the Calculation of Physical Effects - Due to Releases of Hazardous Materials (Liquids and Gases), "Yellow Book." the Committee for the Prevention of Disasters by Hazardous Materials. Director-General for Social Affairs and Employment, The Hague.
Willoughby, A.B., Ullian, I.J., 1988. Analysis of Project PYRO Close-In Overpressure and Impulse Data - 8423-2RR.
Zalosh, R., Weyandt, N., 2005. Hydrogen fuel tank fire exposure burst test - SAE technical paper 2005-01-1886. SAE 2005 World Congress & Exhibition. http://dx.doi.org/10.4271/2005-01-1886.
Zhang, J., Laboureur, D., Liu, Y., Mannan, M.S., 2016. Lessons learned from a supercritical pressure BLEVE in nihon dempa kogyo crystal inc. J. Loss Prev. Process. Ind. 41, 315–322. http://dx.doi.org/10.1016/J.JLP.2016.02.012.
Zhuzhgov, A.V., Krivoruchko, O.P., Isupova, L.A., Mart'yanov, O.N., Parmon, V.N., 2018. Low-temperature conversion of ortho-hydrogen into liquid para-hydrogen: process and catalysts. Review. Catal. Ind. 10, 9–19. http://dx.doi.org/10.1134/S2070050418010117.